

Factor Graphs for Quantum Probabilities

Feb. 7, 2017

Hans-Andrea Loeliger and Pascal O. Vontobel

Abstract—A factor-graph representation of quantum-mechanical probabilities (involving any number of measurements) is proposed. Unlike standard statistical models, the proposed representation uses auxiliary variables (state variables) that are not random variables. All joint probability distributions are marginals of some complex-valued function q , and it is demonstrated how the basic concepts of quantum mechanics relate to factorizations and marginals of q .

I. INTRODUCTION

Factor graphs [2]–[4] and similar graphical notations [5]–[8] are widely used to represent statistical models with many variables. Factor graphs have become quite standard in coding theory [9], but their applications include also communications [10], signal processing [11], [12], combinatorics [13], and much more. The graphical notation can be helpful in various ways, including the elucidation of the model itself and the derivation of algorithms for statistical inference.

In this paper, we show how quantum mechanical probabilities (including, in particular, joint distributions over several measurements) can be expressed in factor graphs that are fully compatible with factor graphs of standard statistical models and error correcting codes. This is not trivial: despite being a statistical theory, quantum mechanics does not fit into standard statistical categories and it is not built on the Kolmogorov axioms of probability theory. Existing graphical representations of quantum mechanics such as Feynman diagrams [14], tensor diagrams [15]–[18], and quantum circuits [19, Chap. 4] do not explicitly represent probabilities, and they are not compatible with “classical” graphical models.

Therefore, this paper is not just about a graphical notation, but it offers a perspective of quantum mechanical probabilities that has not (as far as we know) been proposed before.

In order to introduce this perspective, recall that statistical models usually contain auxiliary variables (also called hidden variables or state variables), which are essential for factorizing the joint probability distribution. For example, a hidden Markov model with primary variables Y_1, \dots, Y_n is defined by a joint probability mass function of the form

$$p(y_1, \dots, y_n, x_0, \dots, x_n) = p(x_0) \prod_{k=1}^n p(y_k, x_k | x_{k-1}), \quad (1)$$

H.-A. Loeliger is with the Department of Information Technology and Electrical Engineering, ETH Zurich, Switzerland. Email: loeliger@isi.ee.ethz.ch

P. O. Vontobel is with the Department of Information Engineering, The Chinese University of Hong Kong. Email: pascal.vontobel@iee.org.

A much abbreviated version of this paper was presented at ISIT 2012 [1].

where X_0, X_1, \dots, X_n are auxiliary variables (hidden variables) that are essential for the factorization (1). More generally, the joint distribution $p(y_1, \dots, y_n)$ of some primary variables Y_1, \dots, Y_n is structured by a factorization of the joint distribution $p(y_1, \dots, y_n, x_0, \dots, x_m)$ with auxiliary variables X_0, \dots, X_m and

$$p(y_1, \dots, y_n) = \sum_{x_0, \dots, x_m} p(y_1, \dots, y_n, x_0, \dots, x_m), \quad (2)$$

where the sum is over all possible values of X_0, \dots, X_m . (For the sake of exposition, we assume here that all variables have finite alphabets.) However, quantum-mechanical joint probabilities cannot, in general, be structured in this way.

We now generalize $p(y_1, \dots, y_n, x_0, \dots, x_m)$ in (2) to an arbitrary complex-valued function $q(y_1, \dots, y_n, x_0, \dots, x_m)$ such that

$$p(y_1, \dots, y_n) = \sum_{x_0, \dots, x_m} q(y_1, \dots, y_n, x_0, \dots, x_m). \quad (3)$$

The purpose of q is still to enable a nice factorization, for which there may now be more opportunities. Note that the concept of marginalization carries over to q ; in particular, all marginals of $p(y_1, \dots, y_n)$ (involving any number of variables) are also marginals of q . However, the auxiliary variables X_0, \dots, X_m are not, in general, random variables, and marginals of q involving one or several of these variables are not, in general, probability distributions.

We will show that this generalization allows natural representations of quantum-mechanical probabilities involving any number of measurements. In particular, the factor graphs of this paper will represent pertinent factorizations of complex-valued functions q as in (3).

This paper is not concerned with physics, but only with the peculiar joint probability distributions that arise in quantum mechanics. However, we will show how the basic concepts and terms of quantum mechanics relate to factorizations and marginals of suitable functions q . For the sake of clarity, we will restrict ourselves to finite alphabets (with some exceptions, especially in Appendix B), but this restriction is not essential. Within this limited scope, this paper may even be used as a self-contained introduction to quantum-mechanical probabilities.

To the best of our knowledge, describing quantum probabilities (and, indeed, any probabilities) by explicitly using a function q as in (3) is new. Nonetheless, this paper is, of course, related to much previous work in quantum mechanics and quantum computation. For example, quantum circuits as in [19, Chap. 4] have natural interpretations in terms of factor

graphs as will be demonstrated in Sections V-B and VIII. Our factor graphs are also related to tensor diagrams [15]–[18], see also Sections II-B and Appendix A. Also related is the very recent work by Mori [20]. On the other hand, quantum Bayesian networks (see, e.g., [21]) and quantum belief propagation (see, e.g., [22]) are not immediately related to our approach since they are not based on (3) (and they lack Proposition 1 in Section II). Finally, we mention that the factor graph representation of this paper is used in [23] for estimating the information rate of certain quantum channels.

The paper is structured as follows. Section II reviews factor graphs and their connection to linear algebra. In Section III, we express elementary quantum mechanics (with a single projection measurement) in factor graphs; we also demonstrate how the Schrödinger picture, the Heisenberg picture, and even an elementary form of Feynman path integrals are naturally expressed in terms of factor graphs. Multiple and more general measurements are discussed in Section IV. Section V addresses partial measurements, decompositions of unitary operators (including quantum circuits), and the emergence of non-unitary operators from unitary interactions. In Section VI, we revisit measurements and briefly address their realization in terms of unitary interactions, and in Section VII, we comment on the origin of randomness. In Section VIII, we further illustrate the use of factor graphs by an elementary introduction to quantum coding. Section IX concludes the main part of the paper.

In Appendix A, we offer some additional remarks on the prior literature. In Appendix B, we briefly discuss the Wigner–Weyl representation, which leads to an alternative factor graph representation. In Appendix C, we outline the extension of Monte Carlo methods to the factor graphs of this paper.

This paper contains many figures of factor graphs that represent some complex function q as in (3). The main figures are Figs. 14, 25, 38, and 47; in a sense, the whole paper is about explaining and exploring these four figures.

We will use standard linear algebra notation rather than the bra-ket notation of quantum mechanics. The Hermitian transpose of a complex matrix A will be denoted by $A^H \triangleq \overline{A}^T$, where A^T is the transpose of A and \overline{A} is the componentwise complex conjugate. An identity matrix will be denoted by I . The symbol “ \propto ” denotes equality of functions up to a scale factor.

II. ON FACTOR GRAPHS

A. Basics

Factor graphs represent factorizations of functions of several variables. We will use Forney factor graphs¹ (also called normal factor graphs) as in [3], [4], [11], where nodes (depicted as boxes) represent factors and edges represent variables. For example, assume that some function $f(x_1, \dots, x_5)$ can be written as

$$f(x_1, \dots, x_5) = f_1(x_1, x_2, x_5) f_2(x_2, x_3) f_3(x_3, x_4, x_5). \quad (4)$$

¹Factor graphs as in [2] represent variables not by edges, but by variable nodes. Adapting Proposition 1 for such factor graphs is awkward.

Henceforth in this paper, “factor graph” means “Forney factor graph”; the qualifier “Forney” (or “normal”) will sometimes be added to emphasize that the distinction matters.

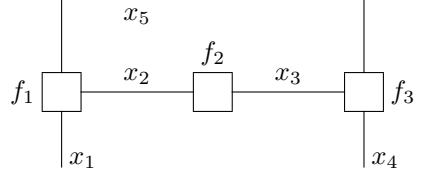


Fig. 1. Factor graph (i.e., Forney factor graph) of (4).

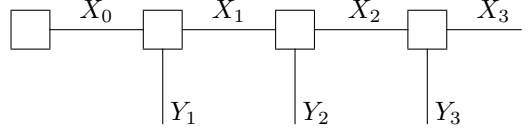


Fig. 2. Factor graph of the hidden Markov model (1) for $n = 3$.

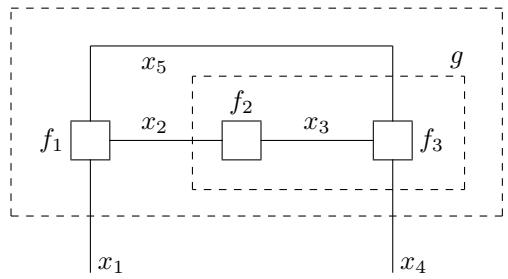


Fig. 3. Closing boxes in factor graphs.

The corresponding factor graph is shown in Fig. 1.

In this paper, all variables in factor graphs take values in finite alphabets (with some exceptions, especially in Appendix B) and all functions take values in \mathbb{C} .

The factor graph of the hidden Markov model (1) is shown in Fig. 2. As in this example, variables in factor graphs are often denoted by capital letters.

The Forney factor-graph notation is intimately connected with the idea of opening and closing boxes [4], [11], [24]. Consider the dashed boxes in Fig. 3. The *exterior function* of such a box is defined to be the product of all factors inside the box, summed over all its internal variables. The exterior function of the inner dashed box in Fig. 3 is

$$g(x_2, x_4, x_5) \triangleq \sum_{x_3} f_2(x_2, x_3) f_3(x_3, x_4, x_5), \quad (5)$$

and the exterior function of the outer dashed box is

$$f(x_1, x_4) \triangleq \sum_{x_2, x_3, x_5} f(x_1, \dots, x_5). \quad (6)$$

The summations in (5) and (6) range over all possible values of the corresponding variable(s).

Closing a box means replacing the box with a single node that represents the exterior function of the box. For example, closing the inner dashed box in Fig. 3 replaces the two nodes/factors $f_2(x_2, x_3)$ and $f_3(x_3, x_4, x_5)$ by the single node/factor (5); closing the outer dashed box in Fig. 3 replaces all nodes/factors in (4) by the single node/factor (6); and

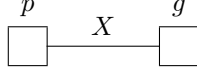


Fig. 4. Factor graph of $E[g(X)]$ according to (8).

closing first the inner dashed box and then the outer dashed box replaces all nodes/factors in (4) by

$$\sum_{x_2, x_5} f_1(x_1, x_2, x_5) g(x_2, x_4, x_5) = f(x_1, x_4). \quad (7)$$

Note the equality between (7) and (6), which holds in general:

Proposition 1. Closing an inner box within some outer box (by summing over the internal variables of the inner box) does not change the exterior function of the outer box. \square

This simple fact is the pivotal property of Forney factor graphs. Closing boxes in factor graphs is thus compatible with marginalization both of probability mass functions and of complex-valued functions q as in (3), which is the basis of the present paper.

Opening a box in a factor graph means the reverse operation of expanding a node/factor into a factor graph of its own.

A *half edge* in a factor graph is an edge that is connected to only one node (such as x_1 in Fig. 1). The *exterior function of a factor graph*² is defined to be the exterior function of a box that contains all nodes and all full edges, but all half edges stick out (such as the outer box in Fig. 3). For example, the exterior function of Fig. 1 is (6). The *partition sum*³ of a factor graph is the exterior function of a box that contains the whole factor graph, including all half edges; the partition sum is a constant.

The exterior function of Fig. 2 is $p(x_n, y_1, \dots, y_n)$, and its partition sum equals one.

Factor graphs can also express expectations: the partition sum (and the exterior function) of Fig. 4 is

$$E[g(X)] = \sum_x p(x)g(x), \quad (8)$$

where $p(x)$ is a probability mass function and g is an arbitrary real-valued (or complex-valued) function.

The equality constraint function $f_=$ is defined as

$$f_=(x_1, \dots, x_n) = \begin{cases} 1, & \text{if } x_1 = \dots = x_n \\ 0, & \text{otherwise.} \end{cases} \quad (9)$$

The corresponding node (which is denoted by “=”) can serve as a branching point in a factor graph (cf. Figs. 21–24): only configurations with $x_1 = \dots = x_n$ contribute to the exterior function of any boxes containing these variables.

A variable with a fixed known value will be marked by a solid square as in Figs. 12 and 23.

²What we here call the exterior function of a factor graph, is called *partition function* in [28]. The term “exterior function” was first used in [27].

³What we call here the partition sum has often been called *partition function*.

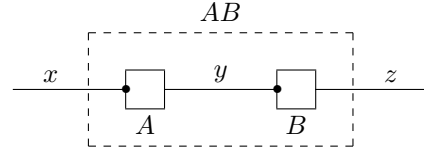


Fig. 5. Factor-graph representation of matrix multiplication (11). The small dot denotes the variable that indexes the rows of the corresponding matrix.

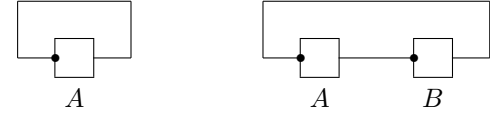


Fig. 6. Factor graph of $\text{tr}(A)$ (left) and of $\text{tr}(AB) = \text{tr}(BA)$ (right).

B. Factor Graphs and Matrices

A matrix $A \in \mathbb{C}^{m \times n}$ may be viewed as a function

$$\{1, \dots, m\} \times \{1, \dots, n\} \rightarrow \mathbb{C} : (x, y) \mapsto A(x, y). \quad (10)$$

The multiplication of two matrices A and B can then be written as

$$(AB)(x, z) = \sum_y A(x, y)B(y, z), \quad (11)$$

which is the exterior function of Fig. 5. Note that the identity matrix corresponds to an equality constraint function $f_=$ (x, y).

In this notation, the trace of a square matrix A is

$$\text{tr}(A) = \sum_x A(x, x), \quad (12)$$

which is the exterior function (and the partition sum) of the factor graph in Fig. 6 (left). Fig. 6 (right) shows the graphical proof of the identity $\text{tr}(AB) = \text{tr}(BA)$.

In this way, closing and opening boxes in factor graphs may thus be viewed as generalizations of matrix multiplication and matrix factorization, respectively.

The factor graph of a diagonal matrix with diagonal elements from some vector v is shown in Fig. 7. Fig. 8 shows the decomposition of a Hermitian matrix A according to the spectral theorem into

$$A = U \Lambda U^H, \quad (13)$$

where U is unitary and where Λ is diagonal and real with diagonal elements from some vector λ .

Factor graphs for linear algebra operations such as Fig. 5 and Fig. 6 (and the corresponding generalizations to tensors) are essentially tensor diagrams (or trace diagrams) as in [18], [25], [26]. This connection between factor graphs and tensor diagrams was noted in [27]–[29] and will further be discussed in Appendix A.

C. Reductions

Reasoning with factor graphs typically involves “local” manipulations of some nodes/factors (such as opening or closing boxes) that preserve the exterior function of all surrounding boxes. Some such reductions are shown in Figs. 9–12; these (very simple) reductions will be essential for understanding the proposed factor graphs for quantum-mechanical probabilities.

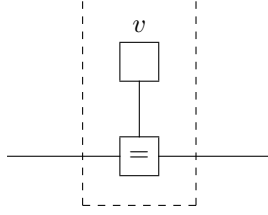


Fig. 7. Factor graph of a diagonal matrix with diagonal vector v . The node labeled “=” represents the equality constraint function (9).

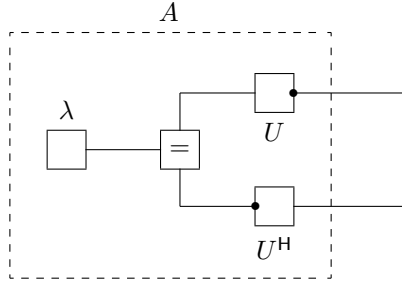


Fig. 8. Factor graph of decomposition (13) according to the spectral theorem.

D. Complex Conjugate Pairs

A general recipe for constructing complex functions q with real and nonnegative marginals as in (3) is illustrated in Fig. 13, where all factors are complex valued. Note that the lower dashed box in Fig. 13 mirrors the upper dashed box: all factors in the lower box are the complex conjugates of the corresponding factors in the upper dashed box. The exterior function of the upper dashed box is

$$g(y_1, y_2, y_3) \triangleq \sum_{x_1, x_2} g_1(x_1, y_1) g_2(x_1, x_2, y_2) g_3(x_2, y_3) \quad (14)$$

and the exterior function of the lower dashed box is

$$\sum_{x'_1, x'_2} \overline{g_1(x'_1, y_1)} \overline{g_2(x'_1, x'_2, y_2)} \overline{g_3(x'_2, y_3)} = \overline{g(y_1, y_2, y_3)}. \quad (15)$$

It follows that closing both boxes in Fig. 13 yields

$$g(y_1, y_2, y_3) \overline{g(y_1, y_2, y_3)} = |g(y_1, y_2, y_3)|^2, \quad (16)$$

which is real and nonnegative.

All factor graphs for quantum-mechanical probabilities that will be proposed in this paper (except in Appendix B) are special cases of this general form. With two parts that are complex conjugates of each other, such representations might seem redundant. Indeed, one of the two parts could certainly be depicted in some abbreviated form; however, as mathematical objects subject to Proposition 1, our factor graphs must contain both parts. (Also, the Monte Carlo methods of Appendix C work with samples where $x'_k \neq x_k$.)

III. ELEMENTARY QUANTUM MECHANICS IN FACTOR GRAPHICS

A. Born's Rule

We begin with an elementary situation with a single measurement as shown in Fig. 14. In this factor graph, $p(x)$ is

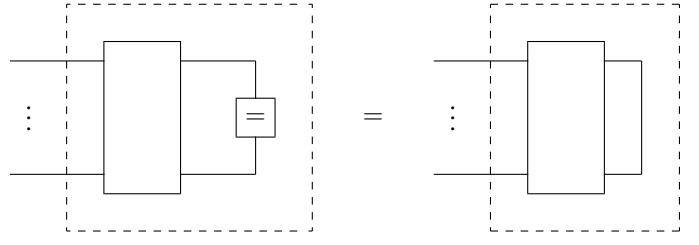


Fig. 9. A two-variable equality constraint (i.e., an identity matrix) can be dropped or added.

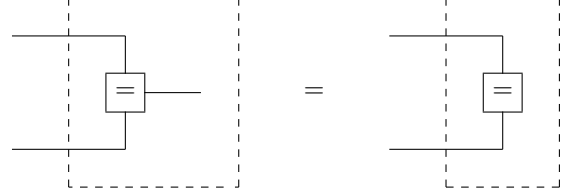


Fig. 10. A half edge out of an equality constraint node (of any degree) can be dropped or added.

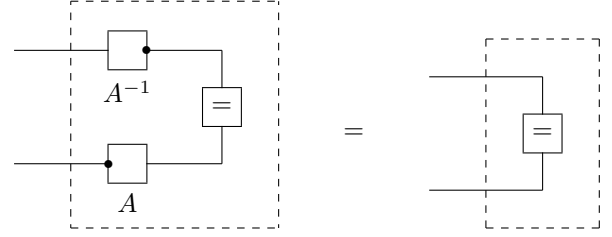


Fig. 11. A regular square matrix A multiplied by its inverse reduces to an identity matrix (i.e., a two-variable equality constraint).

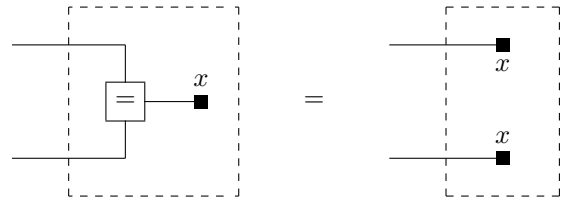


Fig. 12. A fixed known value (depicted as a small solid square) propagates through, and thereby eliminates, an equality constraint.

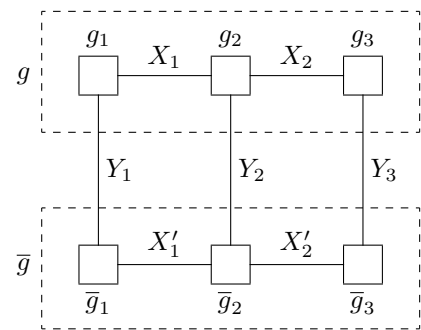


Fig. 13. Factor graph with complex factors and nonnegative real marginal (16).

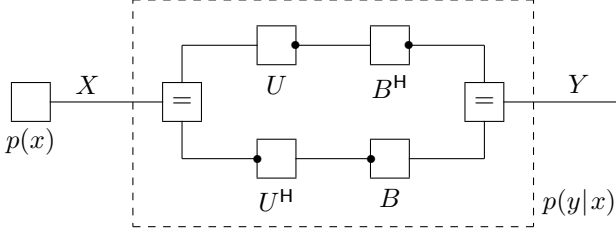


Fig. 14. Factor graph of an elementary quantum system.

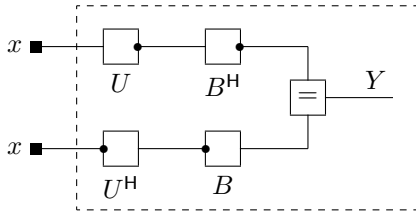


Fig. 15. Dashed box of Fig. 14 for fixed $X = x$. The partition sum of this factor graph equals one.

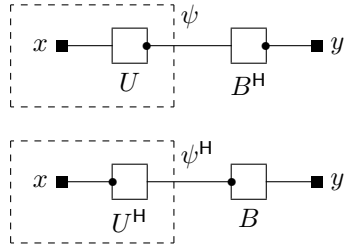


Fig. 16. Derivation of (18) and (19).

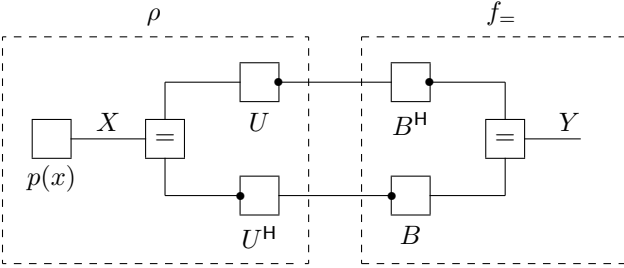


Fig. 17. Regrouping Fig. 14 into a density matrix ρ and an equality constraint $f =$.

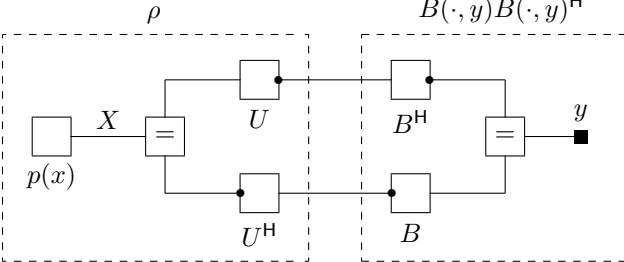


Fig. 18. Fig. 17 for fixed $Y = y$.

a probability mass function, U and B are complex-valued unitary $M \times M$ matrices, and all variables take values in the set $\{1, \dots, M\}$. The matrix U describes the unitary evolution of the initial state X . The matrix B defines the basis for the projection measurement whose outcome is Y (as will further be discussed below). The exterior function of the dashed box is $p(y|x)$, which we will examine below; with that box closed, the factor graph represents the joint distribution

$$p(x, y) = p(x)p(y|x). \quad (17)$$

We next verify that the dashed box in Fig. 14 can indeed represent a conditional probability distribution $p(y|x)$. For fixed $X = x$, this dashed box turns into (all of) Fig. 15 (see Fig. 12). By the reductions from Figures 10 and 11, closing the dashed box in Fig. 15 turns it into an identity matrix. It follows that the partition sum of Fig. 15 is $I(x, x) = 1$ (i.e., the element in row x and column x of an identity matrix), thus complying with the requirement $\sum_y p(y|x) = 1$.

It is then clear from (17) that the partition sum of Fig. 14 equals 1.

For fixed $X = x$ and $Y = y$, the dashed box in Fig. 14 turns into Fig. 16, and $p(y|x)$ is the partition sum of that factor graph. The partition sum of the upper part of Fig. 16 is $B(\cdot, y)^H U(\cdot, x)$, where $U(\cdot, x)$ is column x of U and $B(\cdot, y)$ is column y of B . The partition sum of the lower part of Fig. 16 is $U(\cdot, x)^H B(\cdot, y)$. Therefore, the partition sum of Fig. 16 is the product of these two terms, i.e.,

$$p(y|x) = |B(\cdot, y)^H U(\cdot, x)|^2 \quad (18)$$

$$= |B(\cdot, y)^H \psi|^2, \quad (19)$$

where $\psi \triangleq U(\cdot, x)$ is the quantum state (or the wave function).

With a little practice, the auxiliary Figures 15 and 16 need not actually be drawn and (18) can be directly read off Fig. 14.

B. Density Matrix

Consider Figures 17 and 18, which are regroupings of Fig. 14. The exterior function of the left-hand dashed box in these figures is the density matrix ρ of quantum mechanics, which can be decomposed into

$$\rho = \sum_x p(x) U(\cdot, x) U(\cdot, x)^H \quad (20)$$

(cf. Fig. 8) and which satisfies

$$\text{tr}(\rho) = \sum_x p(x) \text{tr}(U(\cdot, x) U(\cdot, x)^H) \quad (21)$$

$$= \sum_x p(x) \text{tr}(U(\cdot, x)^H U(\cdot, x)) \quad (22)$$

$$= \sum_x p(x) \|U(\cdot, x)\|^2 \quad (23)$$

$$= \sum_x p(x) \quad (24)$$

$$= 1. \quad (25)$$

The exterior function of the right-hand dashed box in Fig. 17 is an identity matrix (i.e., an equality constraint function), as is obvious from the reductions of Figs. 10 and 11. It is

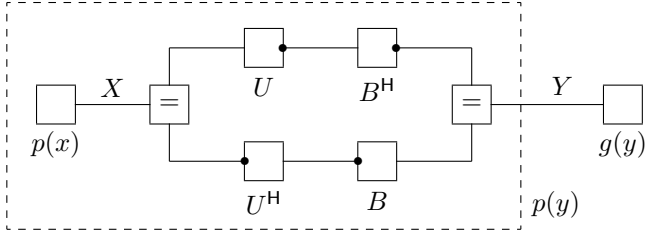


Fig. 19. Factor graph of expectation (29).

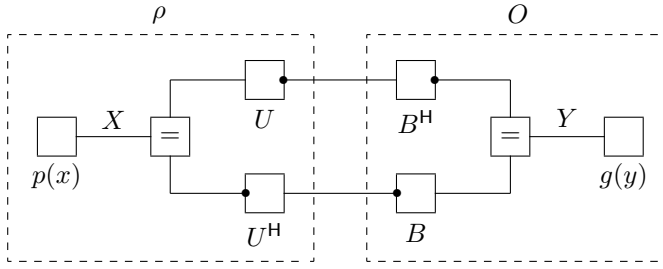


Fig. 20. Factor graph of expectation (30) with general Hermitian matrix O .

then obvious (cf. Fig. 6) that the partition sum of Fig. 17 is $\text{tr}(\rho)$, which equals 1 by (25). (But we already established in Section III-A that the partition sum of Figs. 14 and 17 is 1.)

The exterior function of the right-hand dashed box in Fig. 18 (with fixed $Y = y$) is the matrix $B(\cdot, y)B(\cdot, y)^H$. From Fig. 14, we know that the partition sum of Fig. 18 is $\sum_x p(x, y) = p(y)$. Using Fig. 6, this partition sum can be expressed as

$$p(y) = \text{tr}(\rho B(\cdot, y)B(\cdot, y)^H) \quad (26)$$

$$= \text{tr}(B(\cdot, y)^H \rho B(\cdot, y)) \quad (27)$$

$$= B(\cdot, y)^H \rho B(\cdot, y). \quad (28)$$

Plugging (20) into (28) is, of course, consistent with (18).

C. Observables

In most standard formulations of quantum mechanics, the outcome of a physical experiment is not Y as in Fig. 14, but some (essentially arbitrary) real-valued function $g(Y)$.

In Fig. 19, we have augmented Fig. 14 by a corresponding factor $g(Y)$. The partition sum of Fig. 19 is thus

$$E[g(Y)] = \sum_y p(y)g(y), \quad (29)$$

cf. Fig. 4. Regrouping Fig. 19 as in Fig. 18 yields Fig. 20, the partition sum of which is

$$E[g(Y)] = \text{tr}(\rho O), \quad (30)$$

where the matrix O is the right-hand dashed box in Fig. 18. Note that, by the spectral theorem, every Hermitian matrix O can be represented as in Fig. 20 (cf. Fig. 8) and $g(1), \dots, g(M)$ are the eigenvalues of O .

In this paper, however, we will focus on probabilities and we will not further use such expectations.

D. Evolution over Time: Schrödinger, Heisenberg, Feynman

Consider the factor graph of Fig. 21, which agrees with Fig. 14 except that the matrix U is expanded into the product $U = U_n \cdots U_1$. One interpretation of this factor graph is that the initial state X evolves unitarily over n discrete time steps until it is measured by a projection measurement as in Fig. 14. Note that a continuous-time picture may be obtained, if desired, by a suitable limit with $n \rightarrow \infty$.

In this setting, the so-called Schrödinger and Heisenberg pictures correspond to sequentially closing boxes (from the innermost dashed box to the outermost dashed box) as in Figures 22 and 24, respectively; the former propagates the quantum state ψ (or the density matrix ρ) forward in time while the latter propagates the measurement backwards in time. The resulting probability distribution over Y is identical by Proposition 1.

Both the Schrödinger picture and the Heisenberg picture can be reduced to sum-product message passing in a cycle-free graph as follows. In the Schrödinger picture, assume first that the initial state X is known. In this case, we obtain the cycle-free factor graph of Fig. 23, in which $p(y|x)$ is easily computed by left-to-right sum-product message passing (cf. [2], [4]), which amounts to a sequence of matrix-times-vector multiplications

$$\psi_k = U_k \psi_{k-1} \quad (31)$$

with $\psi_1 \triangleq U_1(\cdot, x)$ (= column x of U_1). The quantities ψ_1, \dots, ψ_n in Fig. 23 are the wave functions propagated up to the corresponding time. Since Fig. 23 consists of two complex conjugate parts, it suffices to carry out these computations for one of the two parts.

If the initial state X is not known, we write

$$p(y) = \sum_x p(x)p(y|x), \quad (32)$$

and each term $p(y|x)$ can be computed as in Fig. 23. This decomposition carries over to the relation

$$\rho_k(x', x'') = \sum_x p(x)\psi_k(x')\psi_k^H(x'') \quad (33)$$

$$= \sum_x p(x)\psi_k(x')\overline{\psi_k(x'')} \quad (34)$$

between the wave function ψ_k and the density matrix ρ_k (see Figures 22 and 23) for $k = 1, \dots, n$.

In the Heisenberg picture (Fig. 24), we can proceed analogously. For any fixed $Y = y$, this value can be plugged into the factors/matrices B and B^H , which turns Fig. 24 into a cycle-free factor graph that looks almost like a time-reversed version of Fig. 23. In consequence, $p(y)$ can be computed by right-to-left sum-product message passing, which again amounts to a sequence of matrix-times-vector multiplications.

Finally, we note that the dashed boxes in Fig. 21 encode Feynman's path integral in its most elementary embodiment. Each internal configuration (i.e., an assignment of values to all variables) in such a box may be viewed as a "path", and the corresponding product of all factors inside the box may be viewed as the (complex) weight of the path. The exterior function of the box is (by definition) the sum, over all internal configurations/paths, of the weight of each configuration/path.

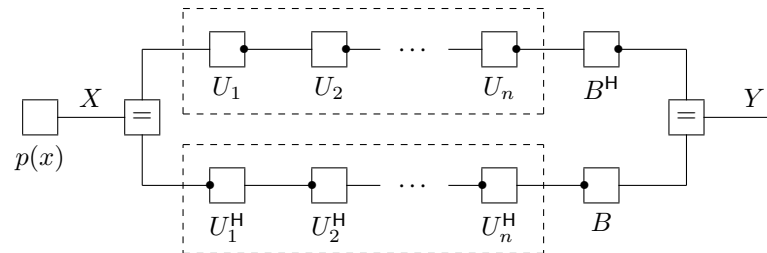


Fig. 21. Elementary quantum mechanics: unitary evolution over time in n steps followed by a single projection measurement.

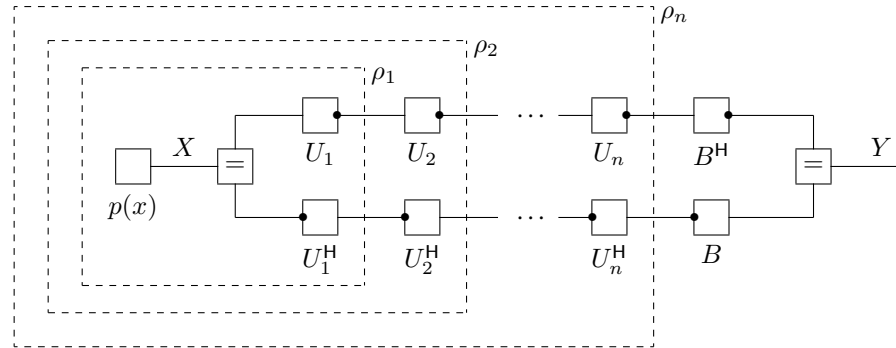


Fig. 22. Schrödinger picture.

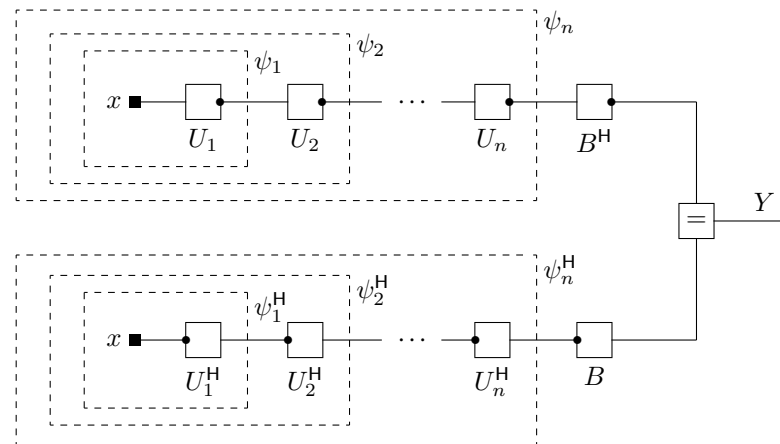


Fig. 23. Schrödinger picture with known initial state $X = x$ and unitarily evolving quantum state (or wave function) ψ .

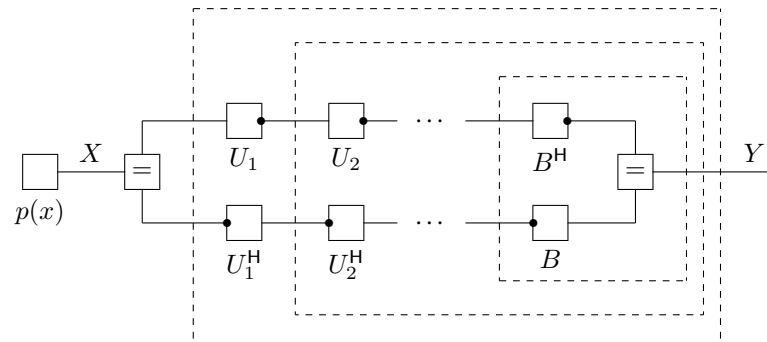


Fig. 24. Heisenberg picture.

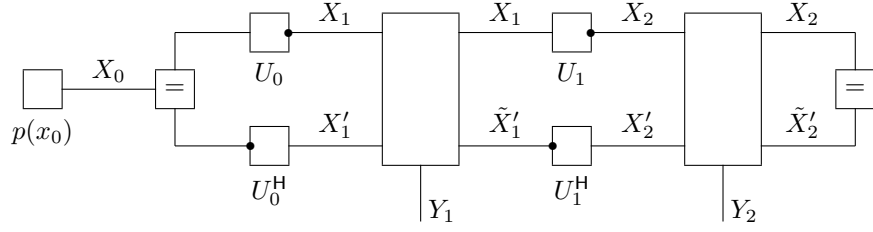


Fig. 25. Factor graph of a quantum system with two measurements and the corresponding observations Y_1 and Y_2 .

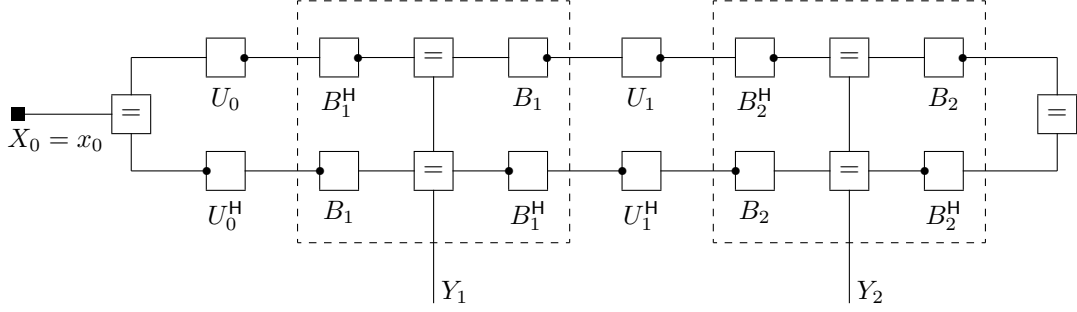


Fig. 26. Important special case of Fig. 25: all matrices are unitary and the initial state $X_0 = x_0$ is known. In quantum-mechanical terms, such measurements are projection measurements with one-dimensional eigenspaces.

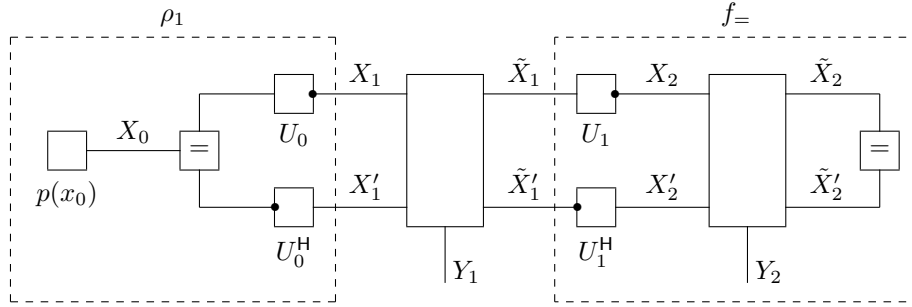


Fig. 27. The exterior function of the dashed box on the left is the density matrix $\rho_1(x_1, x_1')$. The exterior function of the dashed box on the right is $f=(\tilde{x}_1, \tilde{x}_1')$ (assuming that Y_2 is unknown).

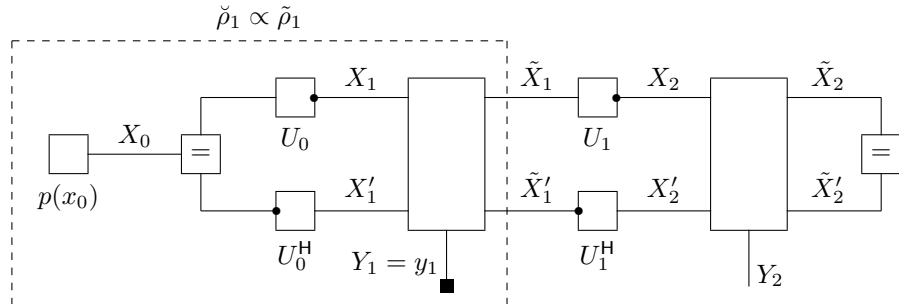


Fig. 28. The exterior function of the dashed box $\check{\rho}_1$ equals the density matrix $\check{\rho}_1$, up to a scale factor, after measuring $Y_1 = y_1$, cf. (40).

IV. MULTIPLE AND MORE GENERAL MEASUREMENTS

We now turn to multiple and more general measurements. Consider the factor graph of Fig. 25. In this figure, U_0 and U_1 are $M \times M$ unitary matrices, and all variables except Y_1 and Y_2 take values in the set $\{1, \dots, M\}$. The two large boxes in the figure represent measurements, as will be detailed below. The factor/box $p(x_0)$ is a probability mass function over the initial state X_0 . We will see that this factor graph (with suitable modeling of the measurements) represents the joint probability mass function $p(y_1, y_2)$ of a general M -dimensional quantum system with two observations Y_1 and Y_2 . The generalization to more observed variables Y_1, Y_2, \dots is obvious.

The unitary matrix U_0 in Fig. 25 represents the development of the system between the initial state and the first measurement according to the Schrödinger equation; the unitary matrix U_1 in Fig. 25 represents the development of the system between the two measurements.

In the most basic case, the initial state $X_0 = x_0$ is known and the measurements look as shown in Fig. 26, where the matrices B_1 and B_2 are also unitary (cf. Fig. 14). In this case, the observed variables Y_1 and Y_2 take values in $\{1, \dots, M\}$ as well. Note that the lower part of this factor graph is the complex conjugate mirror of the upper part (as in Fig. 13).

In quantum-mechanical terms, measurements as in Fig. 26 are projection measurements with one-dimensional eigenspaces (as in Section III).

A very general form of measurement is shown in Fig. 29. In this case, the range of Y_k is a finite set \mathcal{Y}_k , and for each $y_k \in \mathcal{Y}_k$, the factor $A_k(\tilde{x}_k, x_k, y_k)$ corresponds to a complex square matrix $A_k(y_k)$ (with row index \tilde{x}_k and column index x_k) such that

$$\sum_{y_k \in J_k} A_k(y_k)^H A_k(y_k) = I, \quad (35)$$

cf. [19, Chap. 2]. A factor-graphic interpretation of (35) is given in Fig. 30. Condition (35) is both necessary and sufficient for Proposition 2 (below) to hold. Measurements as in Fig. 26 are included as a special case with $\mathcal{Y}_k = \{1, \dots, M\}$ and

$$A_k(y_k) = A_k(y_k)^H = B_k(\cdot, y_k) B_k(\cdot, y_k)^H, \quad (36)$$

where $B_k(\cdot, y_k)$ denotes the y_k -th column of B_k . Note that, for fixed y_k , (36) is a projection matrix.

Measurements will further be discussed in sections V-A and VI.

It is clear from Section II-D that the exterior function of Fig. 25 (with measurements as in Fig. 26 or as in Fig. 29) is real and nonnegative. We now proceed to analyze these factor graphs and to verify that they yield the correct quantum-mechanical probabilities $p(y_1, y_2)$ for the respective class of measurements. To this end, we need to understand the exterior functions of the dashed boxes in Fig. 27. We begin with the dashed box on the right-hand side of Fig. 27.

Proposition 2 (Don't Mind the Future). Closing the dashed box on the right-hand side in Fig. 27 (with a measurement as in Fig. 26 or as in Fig. 29, but with unknown result Y_2 of the measurement) reduces it to an equality constraint function. \square

Proof: For measurements as in Fig. 26, the proof amounts to a sequence of reductions according to Figs. 10 and 11, as illustrated in Fig. 31.

For measurements as in Fig. 29, the key step is the reduction of Fig. 30 to an equality constraint, which is equivalent to the condition (35). \square

Proposition 2 guarantees, in particular, that a future measurement (with unknown result) does not influence present or past observations. The proposition clearly holds also for the extension of Fig. 25 to any finite number of measurements Y_1, Y_2, \dots and can then be applied recursively from right to left.

We pause here for a moment to emphasize this point: it is obvious from Figs. 25 and 26 (generalized to n measurements Y_1, \dots, Y_n) that, in general, a measurement resulting in some variable Y_k affects the joint distribution of all other variables Y_1, \dots, Y_n (both past and future) *even if the result Y_k of the measurement is not known*. By Proposition 2, however, the joint distribution of Y_1, \dots, Y_{k-1} is not affected by the measurement of Y_k, \dots, Y_n provided that no measurement results are known.

Proposition 3 (Proper Normalization). The factor graph of Fig. 25 (with measurements as in Fig. 26 or as in Fig. 29) represents a properly normalized probability mass function, i.e., the exterior function $p(y_1, y_2)$ is real and nonnegative and $\sum_{y_1, y_2} p(y_1, y_2) = 1$. \square

In particular, the partition sum of Fig. 25 equals 1. Again, the proposition clearly holds also for the extension of Fig. 25 to any finite number of measurements Y_1, Y_2, \dots

Proof of Proposition 3: Apply reductions according to Proposition 2 recursively from right to left in Fig. 25, followed by the final reduction $\sum_{x_0} p(x_0) = 1$. \square

Consider now the dashed boxes on the left in Figs. 27 and 28, which correspond to the density matrix before and after measuring Y_1 , respectively. A density matrix ρ is defined to be properly normalized if

$$\text{tr}(\rho) = 1. \quad (37)$$

The dashed box left in Fig. 27 is properly normalized ($\text{tr}(\rho_1) = 1$) by (25). Proper normalization of ρ_k for $k > 1$ follows from Propositions 5–7 below.

Consider next the dashed box in Fig. 28, which we will call $\check{\rho}_1$; it is not a properly normalized density matrix:

Proposition 4 (Trace of the Past).

$$\text{tr}(\check{\rho}_1) = p(y_1); \quad (38)$$

more generally, with k measurements $Y_1 = y_1, \dots, Y_k = y_k$ inside the dashed box, we have

$$\text{tr}(\check{\rho}_k) = p(y_1, \dots, y_k). \quad (39)$$

\square

The proof is immediate from Propositions 2 and 3 (generalized to an arbitrary number of measurements). The properly normalized post-measurement density matrix is then

$$\tilde{\rho}_k \triangleq \check{\rho}_k / p(y_1, \dots, y_k). \quad (40)$$

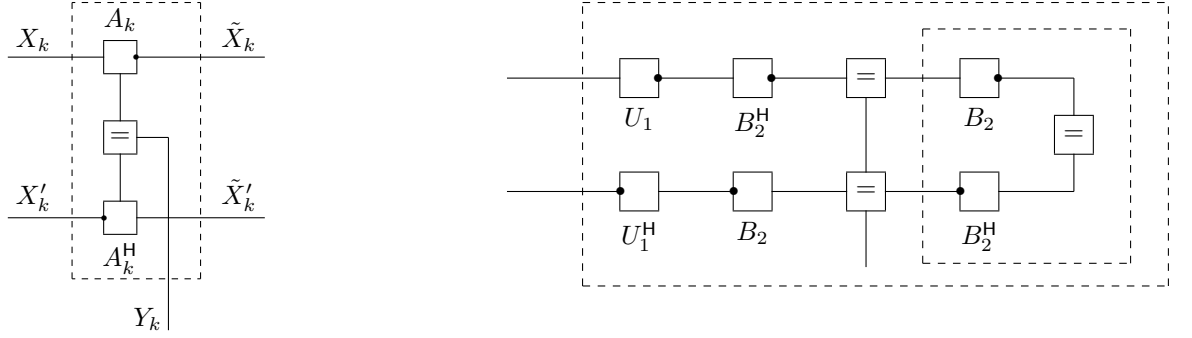


Fig. 29. General measurement as in [19, Chap. 2]. Condition (35) must be satisfied.

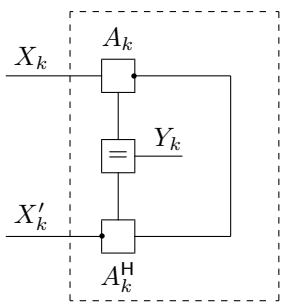


Fig. 30. The dashed box reduces to an equality constraint (i.e., an identity matrix) if and only if (35) holds.

Proposition 5 (Unitary Evolution Between Measurements).

The matrix ρ_{k+1} is obtained from the matrix $\tilde{\rho}_k$ as

$$\rho_{k+1} = U_k \tilde{\rho}_k U_k^H. \quad (41)$$

The proof is immediate from Fig. 5. Note that ρ_{k+1} is properly normalized (provided that $\tilde{\rho}_k$ is so).

Proposition 6 (Basic Projection Measurement). In Fig. 25 (generalized to any number of observations), if Y_k is measured as in Fig. 26, then

$$\begin{aligned}
 P(Y_k=y_k \mid Y_{k-1}=y_{k-1}, \dots, Y_1=y_1) \\
 &= B_k(\cdot, y_k)^H \rho_k B_k(\cdot, y_k) \quad (42) \\
 &= \text{tr}(\rho_k B_k(\cdot, y_k) B_k(\cdot, y_k)^H). \quad (43)
 \end{aligned}$$

After measuring/observing $Y_k = y_k$, the density matrix is

$$\tilde{\rho}_k = B_k(\cdot, y_k) B_k(\cdot, y_k)^H. \quad (44)$$

Note that (44) is properly normalized because

$$\text{tr}(B_k(\cdot, y_k)B_k(\cdot, y_k)^H) = \text{tr}(B_k(\cdot, y_k)^H B_k(\cdot, y_k)) \quad (45)$$

$$= \|B_k(\cdot, y_k)\|^2 = 1. \quad (46)$$

Proof of Proposition 6: For fixed y_1, \dots, y_{k-1} , we have

$$P(Y_k=y_k \mid Y_{k-1}=y_{k-1}, \dots, Y_1=y_1) \\ \propto p(y_k, y_{k-1}, \dots, y_1), \quad (47)$$

where p is the exterior function of Fig. 25 (generalized to any number of observations and with measurements as in Fig. 26).

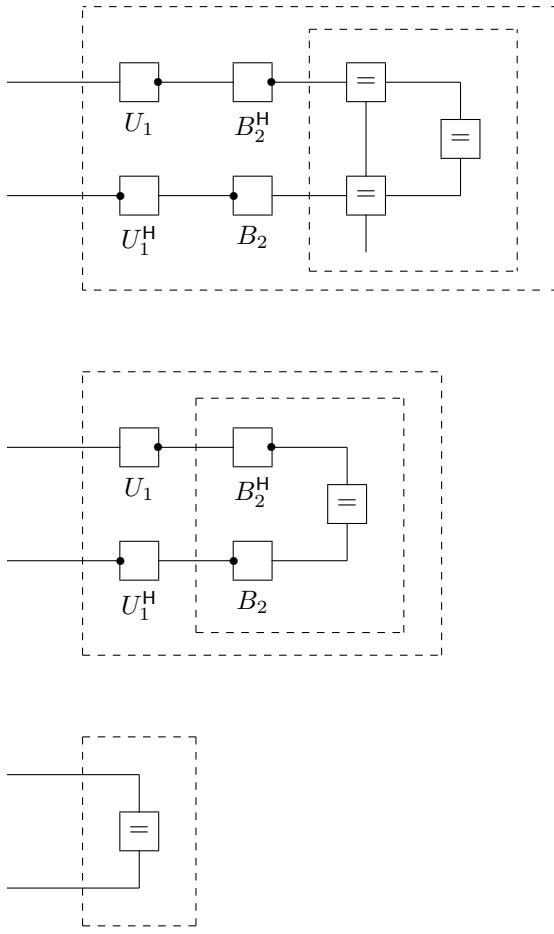


Fig. 31. Proof of Proposition 2 for measurements as in Fig. 26 by a sequence of reductions as in Figs. 11 and 10.

We now reduce Fig. 25 to Fig. 32 as follows: everything to the right of Y_k reduces to an equality constraint according to Proposition 2 (see also Fig. 31), while everything before the measurement of Y_k (with $Y_{k-1} = y_{k-1}, \dots, Y_1 = y_1$ plugged in) is subsumed by ρ_k . Note that the partition sum of Fig. 32 is $\text{tr}(\rho_k) = 1$ (cf. Fig. 17), which means that the exterior function of Fig. 32 equals $p(y_k | y_{k-1}, \dots, y_1)$, i.e., the missing scale factor in (47) has been compensated by the normalization of ρ_k .

For any fixed $Y_k = y_k$, we can then read (42) and (43) from Fig. 32 (cf. Fig. 18).

We now turn to the post-measurement density matrix $\tilde{\rho}_k$. For a measurement $Y_k = y_k$ as in Fig. 26, the dashed box

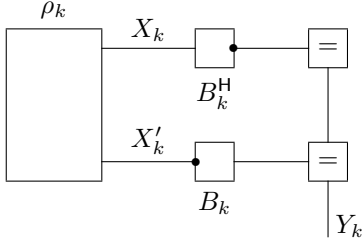
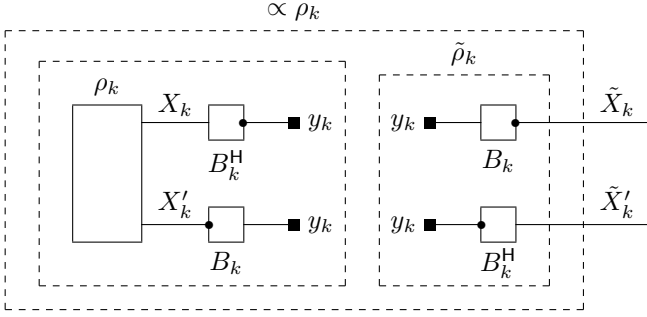
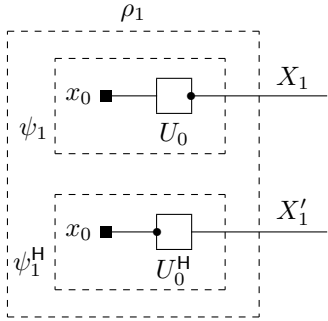


Fig. 32. Proof of Proposition 6: the exterior function equals (42) and (43).

Fig. 33. Proof of Proposition 6: post-measurement density matrix $\tilde{\rho}_k$.Fig. 34. Quantum state ψ_1 .

in Fig. 28 looks as in Fig. 33, which decomposes into two unconnected parts as indicated by the two inner dashed boxes. The exterior function of the left-hand inner dashed box in Fig. 33 is the constant (42); the right-hand inner dashed box equals (44). \square

In the special case of Fig. 26, with known initial state $X_0 = x_0$, the matrix ρ_k factors as

$$\rho_k(x_k, x'_k) = \psi_k(x_k) \overline{\psi_k(x'_k)}, \quad (48)$$

or, in matrix notation,

$$\rho_k = \psi_k \psi_k^H, \quad (49)$$

where ψ_k is a column vector of norm 1. For $k = 1$, we have $\psi_1(x_1) = U_0(x_1, x_0)$, as shown in Fig. 34. The post-measurement density matrix $\tilde{\rho}_k$ factors analogously, as is obvious from (44) or from Fig. 33. In quantum-mechanical terms, ψ_k is the quantum state (cf. Section III). The probability (42) can then be expressed as

$$\begin{aligned} P(Y_k = y \mid Y_{k-1} = y_{k-1}, \dots, Y_1 = y_1) \\ = B_k(\cdot, y)^H \psi_k \psi_k^H B_k(\cdot, y) \end{aligned} \quad (50)$$

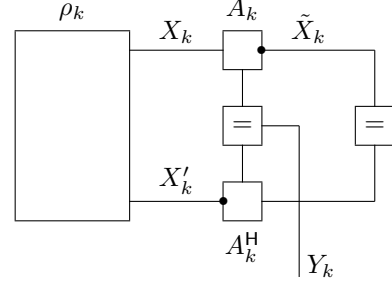


Fig. 35. Proof of Proposition 7: normalization.

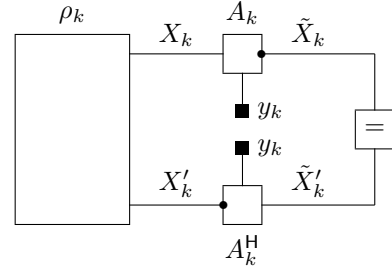
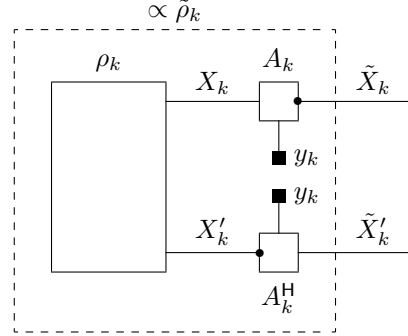


Fig. 36. Proof of Proposition 7: probability (52).

Fig. 37. Proof of Proposition 7: post-measurement density matrix $\tilde{\rho}_k$.

$$= \|B_k(\cdot, y)^H \psi_k\|^2. \quad (51)$$

Proposition 7 (General Measurement). In Fig. 25 (generalized to any number of observations), if Y_k is measured as in Fig. 29, then

$$\begin{aligned} P(Y_k = y_k \mid Y_{k-1} = y_{k-1}, \dots, Y_1 = y_1) \\ = \text{tr}(A_k(y_k) \rho_k A_k(y_k)^H). \end{aligned} \quad (52)$$

After measuring/observing $Y_k = y_k$, the density matrix is

$$\tilde{\rho}_k = \frac{A_k(y_k) \rho_k A_k(y_k)^H}{\text{tr}(A_k(y_k) \rho_k A_k(y_k)^H)} \quad (53)$$

\square

Proof: The proof is parallel to the proof of Proposition 6. For fixed y_{k-1}, \dots, y_1 , we have

$$\begin{aligned} P(Y_k = y_k \mid Y_{k-1} = y_{k-1}, \dots, Y_1 = y_1) \\ \propto p(y_k, y_{k-1}, \dots, y_1), \end{aligned} \quad (54)$$

where p is the exterior function of Fig. 25 (generalized to any number of observations and with measurements as in Fig. 29).

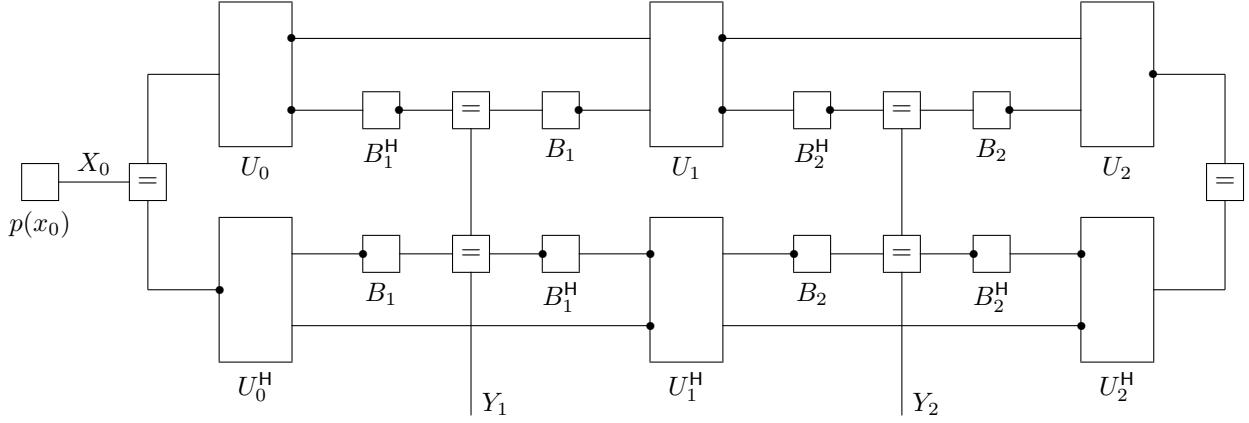


Fig. 38. Factor graph of a quantum system with partial measurements.

We now reduce Fig. 25 to Fig. 35 as follows: everything to the right of Y_k reduces to an equality constraint while everything before the measurement of Y_k (with $Y_{k-1} = y_{k-1}, \dots, Y_1 = y_1$ plugged in) is subsumed by ρ_k . From Fig. 30, we see that the partition sum of Fig. 35 is $\text{tr}(\rho_k) = 1$, which means that the exterior function of Fig. 35 equals $p(y_k|y_{k-1}, \dots, y_1)$, i.e., the missing scale factor in (54) has been compensated by the normalization of ρ_k .

For fixed $Y_k = y_k$, (52) is then obvious from Fig. 36.

Concerning the post-measurement density matrix $\tilde{\rho}_k$, for a measurement $Y_k = y_k$ as in Fig. 29, the dashed box in Fig. 28 looks as in Fig. 37. The numerator of (53) is then obvious from Fig. 37, and the denominator of (53) is simply the proper normalization (37). \square

In summary, Propositions 2–7 verify that the factor graph of Fig. 25 (with measurements as in Fig. 26 or as in Fig. 29) yields the correct quantum-mechanical probabilities for the respective class of measurements.

V. DECOMPOSITIONS AND QUANTUM CIRCUITS, AND NON-UNITARY OPERATORS FROM UNITARY INTERACTIONS

Figs. 25 and 29, while fully general, do not do justice to the richness of quantum-mechanical probabilities and their factor-graphical representation, which we are now going to address.

A. Decompositions and Partial Measurements

Consider the factor graph of Fig. 38. The following points are noteworthy. First, we note that the unitary matrices U_0, U_1, U_2 in Fig. 38 have more than two incident edges. This is to be understood as illustrated in Fig. 39, where the rows of some matrix are indexed by X while its columns are indexed by the pair (V, W) . More generally, rows (marked by a dot) and columns may both be indexed by several variables. Note that, in this way, bundling two unconnected matrices as in Fig. 40 represents the tensor product $A \otimes B$. In Fig. 38, all matrices are square, which implies that the product of the alphabet sizes of the row-indexing variables must equal the product of the alphabet sizes of the column-indexing variables.

Second, each edge in the factor graph of Fig. 38 may actually represent several (finite-alphabet) variables, bundled into a single compound variable.

Third, each of the unitary matrices U_0, U_1, U_2, \dots may itself be a product, either of smaller unitary matrices as illustrated in Fig. 41, or of more general factors as exemplified by Fig. 45; see also Section V-B below.

Forth, it is obvious from Fig. 38 that each measurement involves only some of the variables while some other variables are left alone. The actual measurements shown in Fig. 38 are as in Fig. 26 (with unitary matrices $B_1, B_2 \dots$), but more general measurements could be used.

The measurements in Fig. 38 (including the uninvolved variables) are indeed a special case of measurements as in Fig. 29, as is obvious from Fig. 42, from where we may also read $A_k(y_k) = I \otimes (B_k(y_k)B_k(y_k)^H)$. In order to verify (35), we first recall its factor-graphic interpretation in Fig. 30, which, in this case, amounts to the obvious reduction of Fig. 43 to an equality constraint.

B. Quantum Circuits

Quantum gates [19, Chap. 4] are unitary matrices used in quantum computation. (In Figs. 25 or 38, such quantum gates would appear as, or inside, U_0, U_1, U_2, \dots) For example, Fig. 44 shows a swap gate and Fig. 45 shows a controlled-NOT gate in factor-graph notation. All variables in these two examples are $\{0, 1\}$ -valued (rather than $\{1, 2\}$ -valued), both rows and columns are indexed by pairs of bits (cf. Fig. 39), and the factor f_{\oplus} in Fig. 45 is defined as

$$f_{\oplus} : \{0, 1\}^3 \rightarrow \{0, 1\} : \\ f_{\oplus}(\xi_1, \xi_2, \xi_3) \triangleq \begin{cases} 1, & \text{if } \xi_1 + \xi_2 + \xi_3 \text{ is even} \\ 0, & \text{otherwise.} \end{cases} \quad (55)$$

That Fig. 45 is a unitary matrix may be seen from Fig. 46.

Quantum circuits as in [19, Chap. 4] may then be viewed as, or are easily translated to, the upper half of factor graphs as in Fig. 38. (However, this upper half cannot, by itself, properly represent the joint probability distribution of several measurements.)

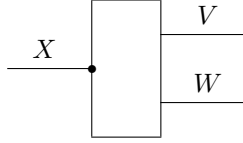


Fig. 39. Matrix with row index X and columns indexed by the pair (V, W) . (E.g., X takes values in $\{0, 1, 2, 3\}$ while V and W are both binary.)

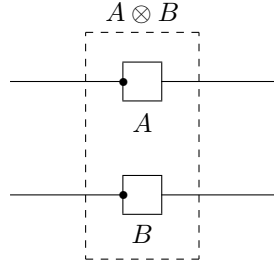


Fig. 40. Tensor product of matrices A and B .

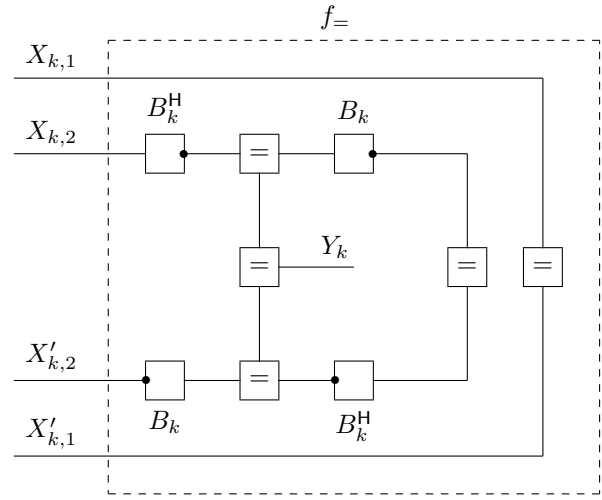


Fig. 43. The exterior function of the dashed box is $f_=(x_{k,1}, x_{k,2}, x'_{k,1}, x'_{k,2}) = f_=(x_{k,1}, x'_{k,1}) f_=(x_{k,2}, x'_{k,2})$.

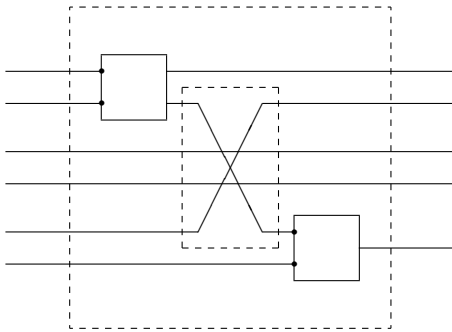


Fig. 41. Decomposition of a unitary matrix into smaller unitary matrices. Line switching as in the inner dashed box is itself a unitary matrix, cf. Fig. 44.

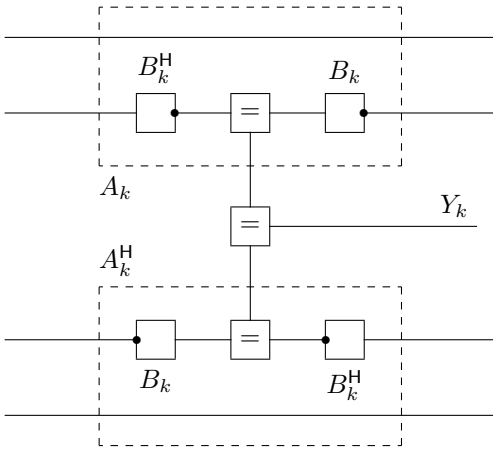


Fig. 42. Measurements in Fig. 38 as a special case of Fig. 29.

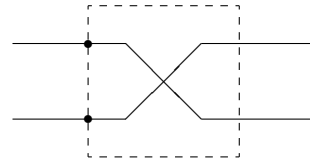


Fig. 44. Swap gate.

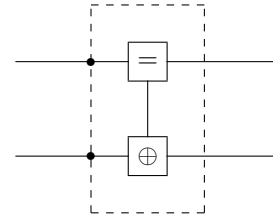


Fig. 45. Controlled-NOT gate.

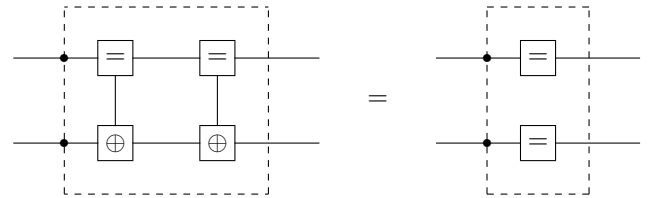


Fig. 46. Proof that Fig. 45 is unitary: the exterior functions left and right are equal.

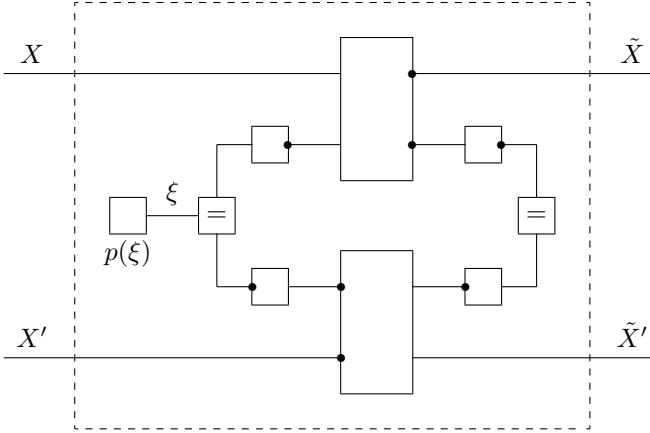


Fig. 47. Two quantum systems interact unitarily. (All unlabeled boxes are unitary matrices.) The resulting exterior function of the dashed box amounts to a measurement with unknown result.

C. Non-unitary Operators from Unitary Interactions

Up to now, we have considered systems composed from only two elements: unitary evolution and measurement. (The role and meaning of the latter continues to be debated, see also Section VI.) However, a natural additional element is shown in Fig. 47, where a primary quantum system interacts once with a secondary quantum system.

(The secondary quantum system might be a stray particle that arrives from “somewhere”, interacts with the primary system, and travels off to somewhere else. Or, with exchanged roles, the secondary system might be a measurement apparatus that interacts once with a particle of interest.)

Closing the dashed box in Fig. 47 does not, in general, result in a unitary operator. In fact, the situation of Fig. 47 may be viewed as a mixture of measurements as in Fig. 29: for any fixed ξ , Fig. 47 represents a measurement as in Fig. 29 except that the result of the measurement is ignored. In other words, marginalizing the secondary system away amounts to a measurement of the primary system (with unknown result).

It seems natural to conjecture that classicality emerges out of such interactions, as has been proposed by Zurek [30], [31] and others.

VI. MEASUREMENTS RECONSIDERED

Our tour through quantum-mechanical concepts followed the traditional route where “measurement” is an unexplained primitive. However, progress has been made in understanding measurement as interaction [32], [33], essentially by reducing it to something like Fig. 47. There thus emerges a view of quantum mechanics fundamentally involving only unitary transforms and marginalization. This view is still imperfectly developed (cf. [33]), but the basic idea can be explained quite easily.

A. Projection Measurements

The realization of a projection measurement by a unitary interaction is exemplified in Fig. 48. As will be detailed below, Fig. 48 (left) is a unitary interaction as in Fig. 47 while Fig. 48

(right) is a projection measurement (with unknown result ζ). We will see that the exterior functions of Fig. 48 (left) and Fig. 48 (right) are equal.

All variables in Fig. 48 (left) take values in the set $\{0, \dots, M-1\}$ (rather than in $\{1, \dots, M\}$) and the box labeled “ \oplus ” generalizes (55) to

$$f_{\oplus} : \{0, \dots, M-1\}^3 \rightarrow \{0, 1\} : \\ f_{\oplus}(\xi_1, \xi_2, \xi_3) \triangleq \begin{cases} 1, & \text{if } (\xi_1 + \xi_2 + \xi_3) \bmod M = 0 \\ 0, & \text{otherwise.} \end{cases} \quad (56)$$

We first note that the two inner dashed boxes in Fig. 48 (left) are unitary matrices, as is easily verified from Fig. 46. Therefore, Fig. 48 (left) is indeed a special case of Fig. 47.

The key step in the reduction of Fig. 48 (left) to Fig. 48 (right) is shown in Fig. 49, which in turn can be verified as follows: the product of the two factors in the box in Fig. 49 (left) is zero unless both

$$\xi + \zeta + \tilde{\xi} = 0 \bmod M \quad (57)$$

and

$$\xi + \zeta' + \tilde{\xi} = 0 \bmod M, \quad (58)$$

which is equivalent to $\zeta = \zeta'$ and (57). For fixed ξ and ζ , (57) allows only one value for $\tilde{\xi}$, which proves the reduction in Fig. 49.

The generalization from fixed ξ to arbitrary $p(\xi)$ is straightforward.

We have thus established that the (marginalized) unitary interaction in Fig. 48 (left) acts like the projection measurement in Fig. 48 (right) and thereby creates the random variable ζ .

Moreover, projection measurements are repeatable, i.e., repeating the same measurement (immediately after the first measurement) leaves the measured quantum system unchanged. (In fact, this property characterizes projection measurements.) Therefore, the random variable ζ is an objective property of the quantum system after the measurement/interaction; it can be cloned, and it can, in principle, be observed via some “channel” $p(y|\zeta)$, as illustrated in Fig. 50.

The conditional-probability factor $p(y|\zeta)$ allows, in particular, that ζ is not fully observable because several values of ζ lead to the same observation Y .

B. General Measurements

A very general form of (indirect) measurement is shown in Fig. 51, which is identical to Fig. 47 except for the observable variable Y . The figure is meant to be interpreted as follows. Some primary quantum system (with variables $X, X', \tilde{X}, \tilde{X}'$) interacts once with a secondary quantum system, which in turn is measured by a projection measurement as in Fig. 50. It is not difficult to verify (e.g., by adapting the procedure in [19, Box 8.1]) that an interaction as in Fig. 51 can realize any measurement as in Fig. 29.

VII. RANDOM VARIABLES RECONSIDERED

Up to Section V, all random variables were either part of the initial conditions (such as X_0 in Fig. 38) or else created by measurements (such as Y_1 and Y_2 in Fig. 38). In Section VI,

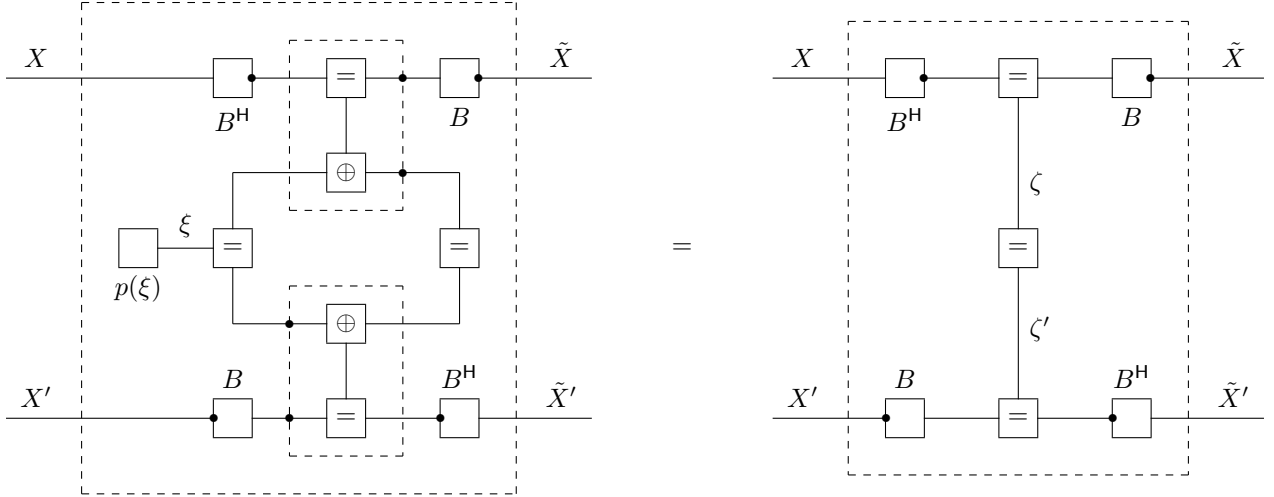


Fig. 48. Projection measurement (with unitary matrix B) as marginalized unitary interaction. Left: unitary interaction as in Fig. 47; the inner dashed boxes are unitary (cf. Fig. 45). Right: resulting projection measurement (with unknown result ζ). The exterior functions left and right are equal.

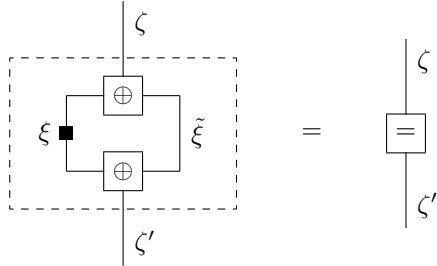


Fig. 49. Proof of the reduction in Fig. 48.

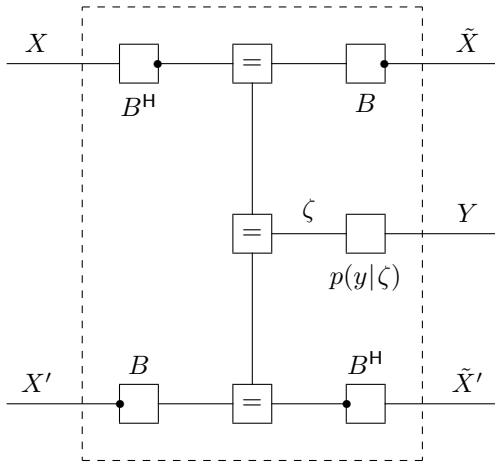


Fig. 50. Observing the post-measurement variable ζ in Fig. 48 (right) via a (classical) ‘channel’ $p(y|\zeta)$.

we have outlined an emerging view of quantum mechanics where measurements are no longer undefined primitives, but explained as unitary interactions.

We now re-examine the creation of random variables in this setting. We find that, fundamentally, random variables are not created by interaction, but by the end of it. The mechanism

is illustrated in Fig. 52: a quantum system with potentially entangled variables (X, X') and (ξ, ξ') splits such that (X, X') and (ξ, ξ') do not interact in the future. In this case, (ξ, ξ') can be marginalized away by closing the dashed box in Fig. 52, which amounts to forming the density matrix $\rho(x, x')$ as a partial trace of $\rho((x, \xi), (x', \xi'))$. In this reduced model, ξ is a random variable (inside the representation of the density matrix $\rho(x, x')$), as is obvious in Fig. 52).

In other words, random variables are created as a byproduct of separation: if a quantum system splits into two parts that do not interact in the future, then focussing on one subsystem (by marginalizing the other subsystem away) turns the state variable(s) of the other subsystem into random variables.

The number of random variables that can be created in this way is limited by the initial state: the product of the alphabet sizes of X and ξ must equal the alphabet size of X_0 in Fig. 52.

In particular, a stochastic process ξ_1, ξ_2, \dots , cannot be created in this way (i.e., without measurements or additional quantum variables) if the alphabet of X_0 is finite.

If we drop the restriction to finite alphabets, then stochastic processes are possible. For example, for $k = 1, 2, 3, \dots$, let

$$X_k = (X_{k,1}, X_{k,2}, \dots) \quad (59)$$

with $X_{k,\ell} \in \{1, \dots, M\}$, let $\xi_k = X_{k,1}$, and let

$$X_{k+1} = (X_{k,2}, X_{k,3}, \dots), \quad (60)$$

as illustrated in Fig. 53. Clearly, ξ_1, ξ_2, \dots is a discrete-time stochastic process generated by a quantum system without measurement.

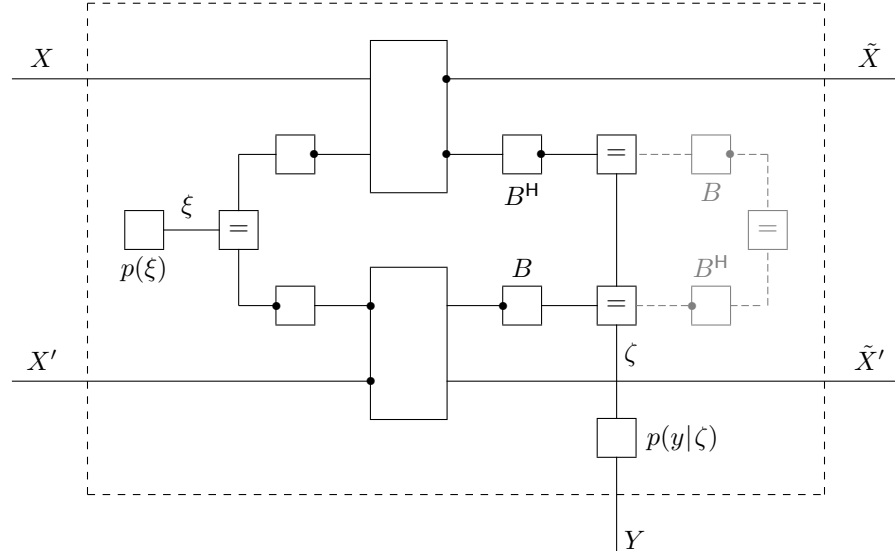


Fig. 51. General measurement as unitary interaction and marginalization. The matrix B and the unlabeled solid boxes are unitary matrices. The part with the dashed edges is redundant.

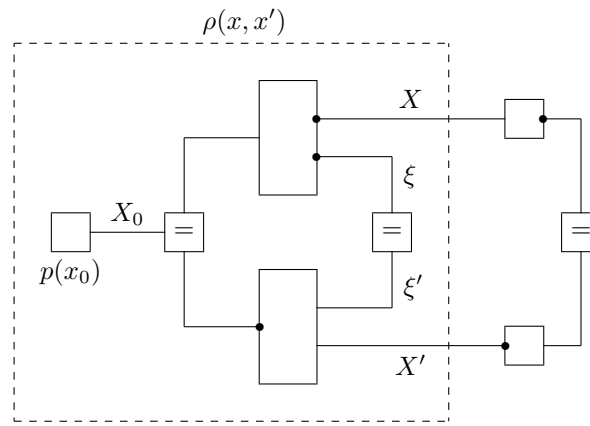


Fig. 52. Marginalization over ξ turns ξ into a random variable. (The unlabeled boxes are unitary matrices.)

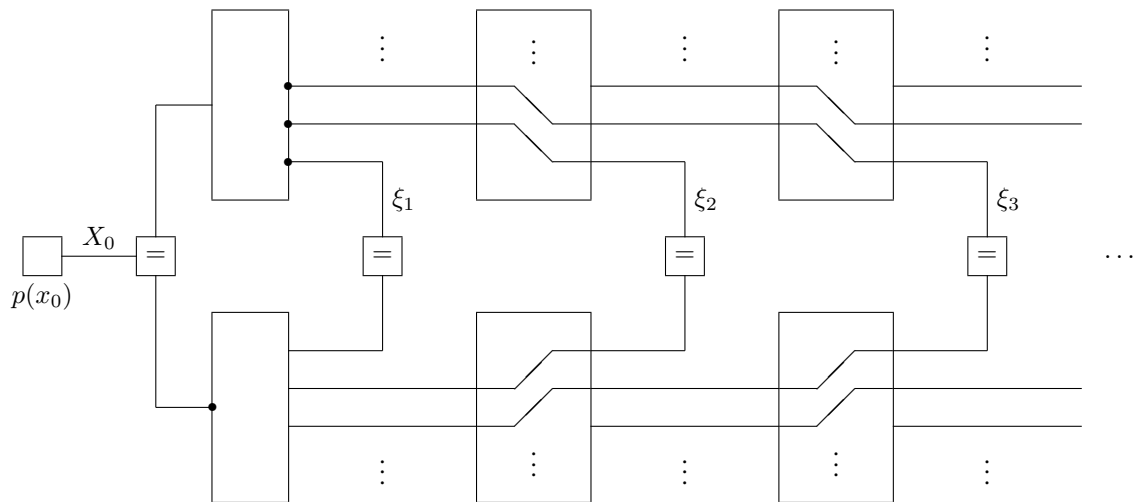


Fig. 53. Stochastic process without measurement. The rectangular boxes are unitary operators.

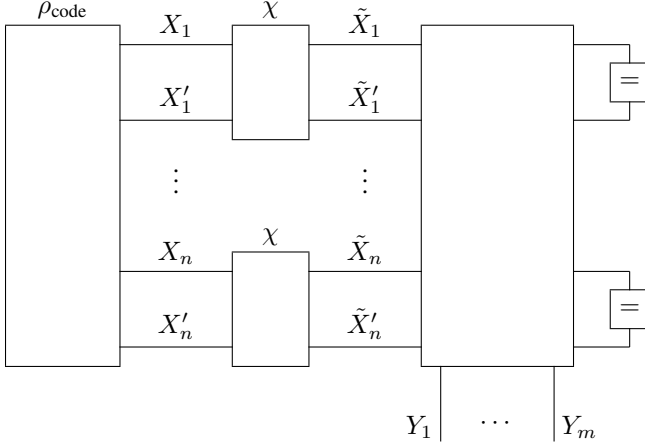


Fig. 54. Factor graph of length- n quantum code, memoryless quantum channel, and detector. Note the visual arrangement of the variables into pairs $(X_1, X'_1), \dots, (X_n, X'_n)$, which differs from most other figures in this paper.

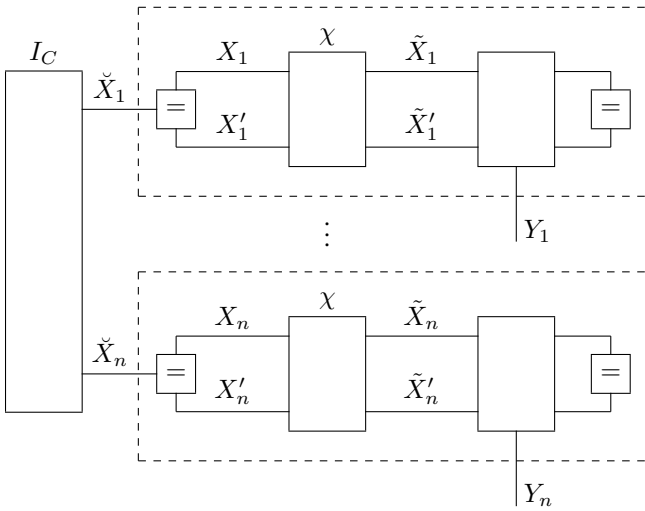


Fig. 55. Quantum channel turned into classical channel and used with classical code with indicator function I_C . (Note the visual arrangement of the variables into pairs $(X_1, X'_1), \dots, (X_n, X'_n)$ as in Fig. 54.)

VIII. ON QUANTUM CODES AND CHANNELS

In this final section, we briefly outline the basic concepts of quantum coding [19] in terms of the factor graph representation.

A quantum channel is an operator that maps a density matrix into another density matrix, as will be discussed below. The purpose of quantum coding is to create an overall quantum system, around the channel, that is insensitive (within some limits) to the action of the channel.

A quantum system with error correction comprises four parts: an encoder, a channel, a detector, and a reconstruction device. The encoder of a quantum code maps some given (classical or quantum) information into a quantum system with state variables $(X_1, X'_1), \dots, (X_n, X'_n)$, which is fed as input to the quantum channel. The output of the quantum channel is processed by the detector, which involves measurements with results Y_1, \dots, Y_m . From these results, the reconstruction

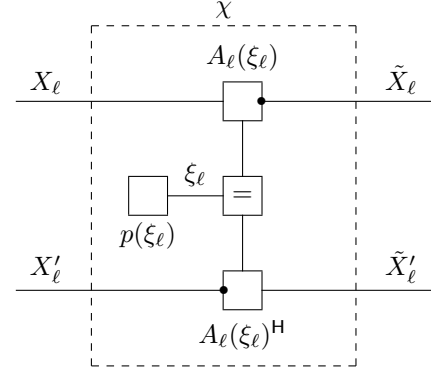


Fig. 56. Factor graph of a general channel model (for use in Fig. 54). The node/factor $p(\xi_\ell)$ may be missing.

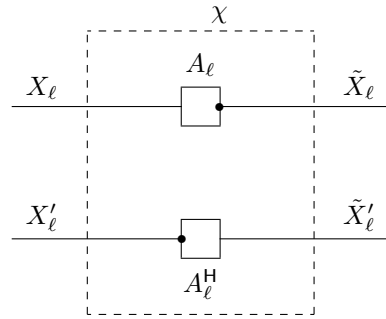


Fig. 57. Simplified version of Fig. 56 for fixed ξ_ℓ .

device attempts to recover either the pre-channel quantum state or the (classical or quantum) information that was encoded.

Fig. 54 shows the factor graph of such a system. More precisely, the figure shows the factor graph of a general code with density matrix ρ_{code} , a memoryless channel, and a general detector. A channel is called memoryless if it operates separately on X_1, X_2, \dots , as shown in Fig. 54. The reconstruction device is not shown in Fig. 54.

In the special case where the code and the detector can be represented as in Fig. 55, the quantum channel is effectively transformed into a classical memoryless channel with $m = n$ and

$$p(y_1, \dots, y_n | \check{x}_1, \dots, \check{x}_n) = \prod_{\ell=1}^n p(y_\ell | \check{x}_\ell), \quad (61)$$

and ρ_{code} effectively reduces to the indicator function

$$I_C(\check{x}_1, \dots, \check{x}_n) \triangleq \begin{cases} 1, & (\check{x}_1, \dots, \check{x}_n) \in C \\ 0, & \text{otherwise} \end{cases} \quad (62)$$

of a classical code C (up to a scale factor). In this case, standard classical decoding algorithms can be used. For example, if C is a low-density parity-check code, it can be decoded by iterative sum-product message passing in the factor graph of C [4], [9].

By contrast, in genuine quantum coding, the detector does not split as in Fig. 55.

A. On Channels

A factor graph of a quite general class of memoryless channel models is shown in Fig. 56, which may be interpreted

in several different ways. For example, the matrix $A_\ell(\xi_\ell)$ might be an unknown unitary matrix that is selected by the random variable ξ_ℓ with probability density function $p(\xi_\ell)$. Or, in an other interpretation, Fig. 56 without the node/factor $p(\xi_\ell)$ is a general measurement as in Fig. 29 with unknown result ξ .

Many quantum coding schemes distinguish only between “no error” in position ℓ (i.e., $A_\ell(\xi_\ell) = I$) and “perhaps some error” (where $A_\ell(\xi_\ell)$ is arbitrary, but nonzero); no other distinction is made and no prior $p(\xi_\ell)$ is assumed. For the analysis of such schemes, Fig. 56 can often be replaced by the simpler Fig. 57. In such an analysis, it may be helpful to express the (fixed, but unknown) matrix A_ℓ in Fig. 57 in some pertinent basis. For example, any matrix $A \in \mathbb{C}^{2 \times 2}$ can be written as

$$A = \sum_{k=0}^3 w_k \sigma_k \quad (63)$$

with $w_0, \dots, w_3 \in \mathbb{C}$ and where $\sigma_0, \dots, \sigma_3$ are the Pauli matrices

$$\sigma_0 \triangleq \begin{pmatrix} 1 & 0 \\ 0 & 1 \end{pmatrix}, \quad (64)$$

$$\sigma_1 \triangleq \begin{pmatrix} 0 & 1 \\ 1 & 0 \end{pmatrix}, \quad (65)$$

$$\sigma_2 \triangleq \begin{pmatrix} 0 & -i \\ i & 0 \end{pmatrix}, \quad (66)$$

and

$$\sigma_3 \triangleq \begin{pmatrix} 1 & 0 \\ 0 & -1 \end{pmatrix}. \quad (67)$$

The matrices $\sigma_0, \dots, \sigma_3$ are unitary and Hermitian, and they form a basis of $\mathbb{C}^{2 \times 2}$.

B. Repeat Codes of Length 2 and 3

Fig. 58 (left) shows the factor graph of an encoder of a simple code of length $n = 3$. All variables in this factor graph are binary, and the initial density matrix ρ_0 is arbitrary. Note that this encoder can be realized with two controlled-not gates (cf. Fig. 45) and two ancillary qubits with fixed initial state zero.

A detector for this code is shown in Fig. 58 (right). This detector can be realized with two controlled-not gates and two qubit measurements. The unitary part of this detector inverts the unitary part of the encoder, and the measured bits Y_1 and Y_2 (henceforth called syndrome bits) correspond to the ancillary qubits in the encoder.

The code of Fig. 58 is not very useful in itself, but it suffices to demonstrate some basic ideas of quantum coding and it further illustrates the use of factor graphs. Moreover, once this simple code is understood, it is easy to proceed to the Shor code [19], which can correct an arbitrary single-qubit error.

The encoder-detector pair of Fig. 58 may be viewed as two nested encoder-detector pairs for a repeat code of length $n = 2$: the inner encoder-detector pair produces the syndrome bit Y_2 , and the outer encoder-detector pair produces the syndrome bit Y_1 .

Therefore, we now consider the net effect of the encoder, the channel, and the detector of a repeat code of length $n = 2$ as shown in Figures 59 and 60. We assume that at most one qubit error occurs, either in the direct path (as in Fig. 59) or in the check path (as in Fig. 60). This single potential error is a general nonzero matrix $A \in \mathbb{C}^{2 \times 2}$ (as in Fig. 57) with row and column indices in $\{0, 1\}$.

For fixed $Y = y$, the net effect of the encoder, the channel, and the detector amounts to a matrix $A_=(y)$ or $A_+(y)$ corresponding to the dashed boxes in Figures 59 and 60, respectively.

If $A = I$ (i.e., if there is no error), we necessarily have $Y = 0$ and $A_=(0) = A_+(0) = I$. For general nonzero A , parameterized as in (63), we have

$$A_=(0) = \begin{pmatrix} A(0, 0) & 0 \\ 0 & A(1, 1) \end{pmatrix} \quad (68)$$

$$= w_0 \sigma_0 + w_3 \sigma_3, \quad (69)$$

i.e., the projection of A onto the space spanned by σ_0 and σ_3 , and

$$A_=(1) = \begin{pmatrix} 0 & A(0, 1) \\ A(1, 0) & 0 \end{pmatrix} \quad (70)$$

$$= w_1 \sigma_1 + w_2 \sigma_2, \quad (71)$$

i.e., the projection of A onto the space spanned by σ_1 and σ_2 . Moreover,

$$A_+(0) = A_=(0), \quad (72)$$

and

$$A_+(1) = \begin{pmatrix} A(1, 0) & 0 \\ 0 & A(0, 1) \end{pmatrix} \quad (73)$$

$$= \sigma_1 A_=(1) \quad (74)$$

$$= w_1 \sigma_0 + w_2 i \sigma_3. \quad (75)$$

We now return to Fig. 58, which we consider as two nested encoder-detector pairs as in Figures 59 and 60. We assume that at most one qubit error occurs, or, equivalently, $A_\ell = I$ except for a single index $\ell \in \{1, 2, 3\}$. For the inner encoder-detector pair, the above analysis of Figures 59 and 60 applies immediately. For the outer encoder-detector pair, the same analysis can be reused, with the error matrix A replaced by $A_=(y_2)$ or $A_+(y_2)$ from the inner code. The resulting effective channel from the encoder input to the detector output in Fig. 58, as a function of Y_1 and Y_2 , is tabulated in Table I.

From Table I, we observe that the syndrome bits Y_1 and Y_2 uniquely determine the resulting effective channel, which allows us to compress Table I into Table II. Note that the four unknown parameters w_0, w_1, w_2, w_3 of the error matrix (63) are thus converted into only two unknown parameters (either w_0 and w_3 or w_1 and w_2 , depending on Y_1, Y_2).

In the special case where we consider only bit flips, i.e., if we assume $w_2 = w_3 = 0$, then it is obvious from Table II that the code of Fig. 58 can correct a single bit flip in any position. In fact, from Table I, we see that a bit flip in qubit 1 is manifested in the syndrome $Y_1 = Y_2 = 1$ while a bit flip in qubit 2 or in qubit 3 has no effect on the resulting effective channel, except for an irrelevant scale factor. However, we wish to be able to deal with more general errors.

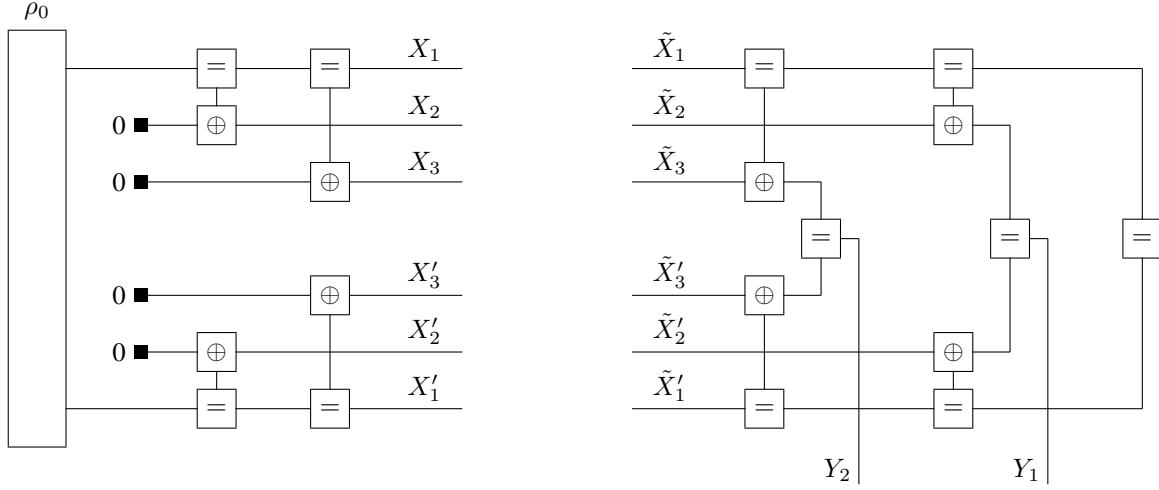


Fig. 58. An encoder (left) and a detector (right) for a repeat code of length $n = 3$.

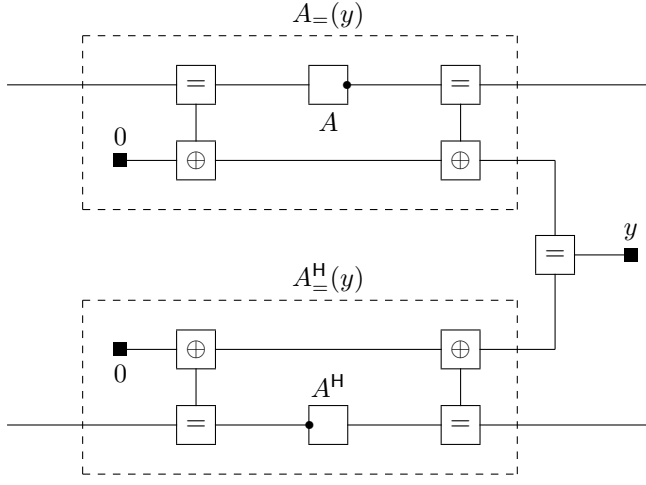


Fig. 59. Effective channel (created by encoder, channel, and detector) of repeat code of length $n = 2$ with an error in the direct path.

TABLE I
NET EFFECT OF ENCODER AND DETECTOR OF FIG. 58 IF AT MOST ONE QUBIT ERROR OCCURS. BOTH THE SINGLE-QUBIT ERROR AND THE RESULTING EFFECTIVE CHANNEL ARE PARAMETERIZED AS IN (63).

Y_2	Y_1	error location		
		1	2	3
0	0	$w_0\sigma_0 + w_3\sigma_3$	$w_0\sigma_0 + w_3\sigma_3$	$w_0\sigma_0 + w_3\sigma_3$
0	1	impossible	$w_1\sigma_0 + w_2i\sigma_3$	impossible
1	0	impossible	impossible	$w_1\sigma_0 + w_2i\sigma_3$
1	1	$w_1\sigma_1 + w_2\sigma_2$	impossible	impossible

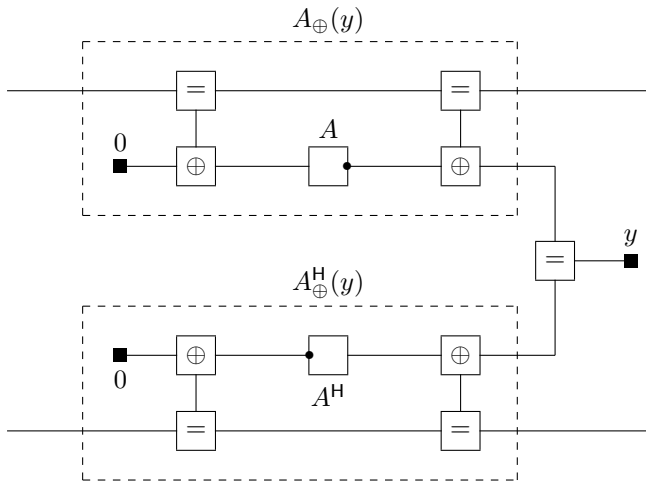


Fig. 60. Effective channel (created by encoder, channel, and detector) of repeat code of length $n = 2$ with an error in the check path.

TABLE II
COMPRESSED VERSION OF TABLE I.

Y_2	Y_1	effective channel
0	0	$w_0\sigma_0 + w_3\sigma_3$
0	1	$w_1\sigma_0 + w_2i\sigma_3$
1	0	$w_1\sigma_0 + w_2i\sigma_3$
1	1	$w_1\sigma_1 + w_2\sigma_2$

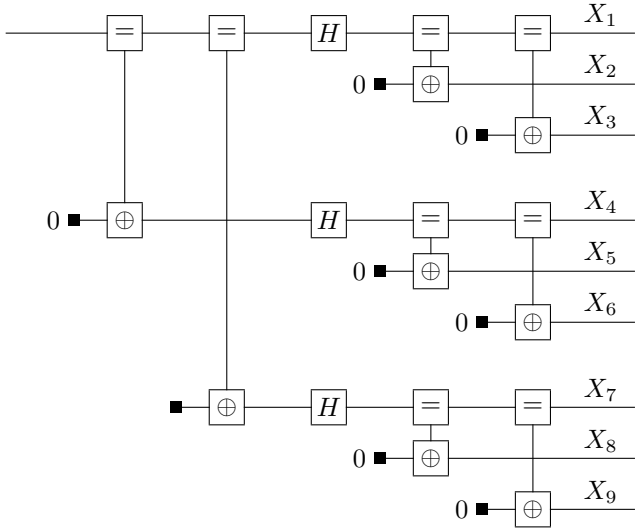


Fig. 61. Encoder of the Shor code. The figure shows only the upper half of the factor graph (i.e., the quantum circuit). The nodes labeled “H” represent the normalized Hadamard matrix

$$H \triangleq \frac{1}{\sqrt{2}} \begin{pmatrix} 1 & 1 \\ 1 & -1 \end{pmatrix}, \quad (76)$$

which is symmetric and unitary and satisfies $H\sigma_1 = \sigma_3H$, and $H\sigma_2 = -\sigma_2H$. Note that this encoder uses four copies of the encoder in Fig. 58: three independent inner encoders are glued together with an outer encoder.

As a detector, we use the obvious generalization of Fig. 58 (right), i.e., the mirror image of the encoder.

This encoder-detector pair is easily analyzed using the results of Section VIII-B. For this analysis, we assume that at most a single qubit error occurs (i.e., $A_\ell \neq I$ for at most one index $\ell \in \{1, \dots, 9\}$). In consequence, two of the three inner encoder-detector pairs are error-free and reduce to an identity matrix. The remaining inner encoder-detector pair is described by Table II. The multiplication by H both in the encoder and in the detector changes Table II to Table III. Note that the resulting effective channel is either of the form $a\sigma_0 + b\sigma_1$ or $c\sigma_2 + d\sigma_3$, and the detector knows which case applies.

The outer encoder-detector pair thus sees an error in at most one position, and the potential error is described by Table II, except that the underlying channel is not (63), but as in Table III. Revisiting Table II accordingly yields Table IV, which describes the net effect of the outer encoder-detector pair. In any case, the resulting effective channel is of the form $\alpha\sigma_k$ for some nonzero $\alpha \in \mathbb{C}$ and some (known) $k \in \{0, 1, 2, 3\}$. In other words, the effective channel (from encoder input to detector output) is fully determined by the 8 syndrome bits, up to an irrelevant scale factor. In consequence, the (arbitrary) original quantum state can exactly be restored.

TABLE III
EFFECTIVE CHANNEL OF TABLE II
WITH PRE- AND POST-MULTIPLICATION BY H .

Y_2	Y_1	effective channel
0	0	$w_0\sigma_0 + w_3\sigma_1$
0	1	$w_1\sigma_0 + w_2i\sigma_1$
1	0	$w_1\sigma_0 + w_2i\sigma_1$
1	1	$w_1\sigma_3 - w_2\sigma_2$

TABLE IV
NET EFFECT OF ENCODER (AS IN FIG. 61) AND MIRROR-IMAGE DETECTOR
OF SHOR CODE, ASSUMING THAT AT MOST ONE QUBIT ERROR OCCURS.
“INNER CODE” REFERS TO THE INNER ENCODER-DETECTOR PAIR WITH
THE POTENTIAL ERROR.

outer detector Y_2	Y_1	effect of inner code	
		$a\sigma_0 + b\sigma_1$	$c\sigma_2 + d\sigma_3$
0	0	$a\sigma_0$	$d\sigma_3$
0	1	$b\sigma_0$	$ci\sigma_3$
1	0	$b\sigma_0$	$ci\sigma_3$
1	1	$b\sigma_1$	$c\sigma_2$

IX. CONCLUSION

We have proposed factor graphs for quantum-mechanical probabilities involving any number of measurements, both for basic projection measurements and for general measurements. Our factor graphs represent factorizations of complex-valued functions q as in (3) such that the joint probability distribution of all random variables (in a given quantum system) is a marginal of q . Therefore (and in contrast to other graphical representations of quantum mechanics), our factor graphs are fully compatible with standard statistical models. We have also interpreted a variety of concepts and quantities of quantum mechanics in terms of factorizations and marginals of such functions q . We have further illustrated the use of factor graphs by an elementary introduction to quantum coding.

In Appendix A, we offer some additional remarks on the prior literature. In Appendix B, we derive factor graphs for the Wigner–Weyl representation. In Appendix C, we point out that the factor graphs of this paper are amenable (at least in principle) to Monte Carlo algorithms.

We hope that our approach makes quantum-mechanical probabilities more accessible to non-physicists and further promotes the exchange of concepts and algorithms between physics, statistical inference, and error correcting codes in the spirit of [5], [24], [34].

APPENDIX A ADDITIONAL REMARKS ABOUT RELATED WORK

A. Tensor Networks

With hindsight, the factor graphs of this paper are quite similar to tensor networks [16]–[18], which have recently moved into the heart of theoretical physics [34].

Tensor networks (and related graphical notation) have been used to represent the wave function $|\Psi\rangle$ of several entangled spins at a given time. In general, the resulting states are called tensor network states (TNS), but depending on the structure of the tensor network, more specialized names like matrix product states (MPS), tree tensor states (TTS), etc., are used. A very nice overview of this line of work is given in the survey paper by Cirac and Verstraete [16], which also explains the connection of TNS to techniques like the density matrix renormalization group (DMRG), the multiscale entanglement renormalization ansatz (MERA), and projected entangled pair states (PEPS).

If such tensor diagrams are used to represent quantities like $\langle\Psi|\Psi\rangle$ or $\langle\Psi|\sigma_2\sigma_4|\Psi\rangle$ (see, e.g., Fig. 2 in [16]), they have two conjugate parts, like the factor graphs in the present paper (Fig. 13 etc.).

It should be noted, however, that the graphical conventions of tensor networks differ from factor graphs in this point: the meaning of a tensor network diagram frequently depends on its orientation on the page (see, e.g., [18]), and exchanging left and right amounts to a transposition, as illustrated in Fig. 62.

B. Quantum Bayesian Networks and Quantum Belief Propagation

Whereas the present paper uses conventional Forney factor graphs (with standard semantics and algorithms), various



Fig. 62. Tensor network notation. Left: bra (row vector); right: ket (column vector). Note that the meaning of the symbol depends on its orientation on the page.

authors have proposed modified graphical models or specific “quantum algorithms” for quantum mechanical quantities [21], [35], [36]. Such graphical models (or algorithms) are not compatible with standard statistical models.

C. Keldysh Formalism

There are some high-level similarities between the graphical models in the present paper and some diagrams that appear in the context of the Keldysh formalism (see, e.g., [37]); in particular, both have “two branches along the time axis.”

However, there are also substantial dissimilarities: first, the diagrams in the Keldysh formalism also have a third branch along the imaginary axis; second, our factor graphs are arguably more explicit than the diagrams in the Keldysh formalism.

D. Normal Factor Graphs, Classical Analytical Mechanics, and Feynman Path Integrals

In [38], it is shown how Forney factor graphs (= normal factor graphs) can be used for computations in classical analytical mechanics. In particular, it is shown how to represent the action $S(x)$ of a trajectory x and how to use the stationary-sum algorithm for finding the path where the action is stationary.

It is straightforward to modify the factor graphs in [38] in order to compute, at least in principle, Feynman path integrals, where $\exp(\frac{i}{\hbar}S(x))$ is integrated over a suitable domain of paths x : essentially by replacing the function nodes $f(\cdot)$ in [38] by $\exp(\frac{i}{\hbar}f(\cdot))$, and by replacing the stationary-sum algorithm by standard sum-product message passing [4].

APPENDIX B WIGNER–WEYL REPRESENTATION

The Wigner–Weyl representation of quantum mechanics expresses the latter in terms of the “phase-space” coordinates \mathbf{q} and \mathbf{p} (corresponding to the position and the momentum, respectively, of classical mechanics). When transformed into this representation, the density matrix turns into a real-valued function.

So far in this paper, all variables were assumed to take values in some finite set without any structure. However, the Wigner–Weyl representation requires that both the original coordinates X and X' and the new coordinates \mathbf{p} and \mathbf{q} can be added and subtracted and admit a Fourier transform as in (80) and (84) below. In the following, we assume $X_k, X'_k, \mathbf{p}_k, \mathbf{q}_k \in \mathbb{R}^N$ for all k .

In a factor graph with continuous variables, the exterior function of a box is defined by integrating over the internal

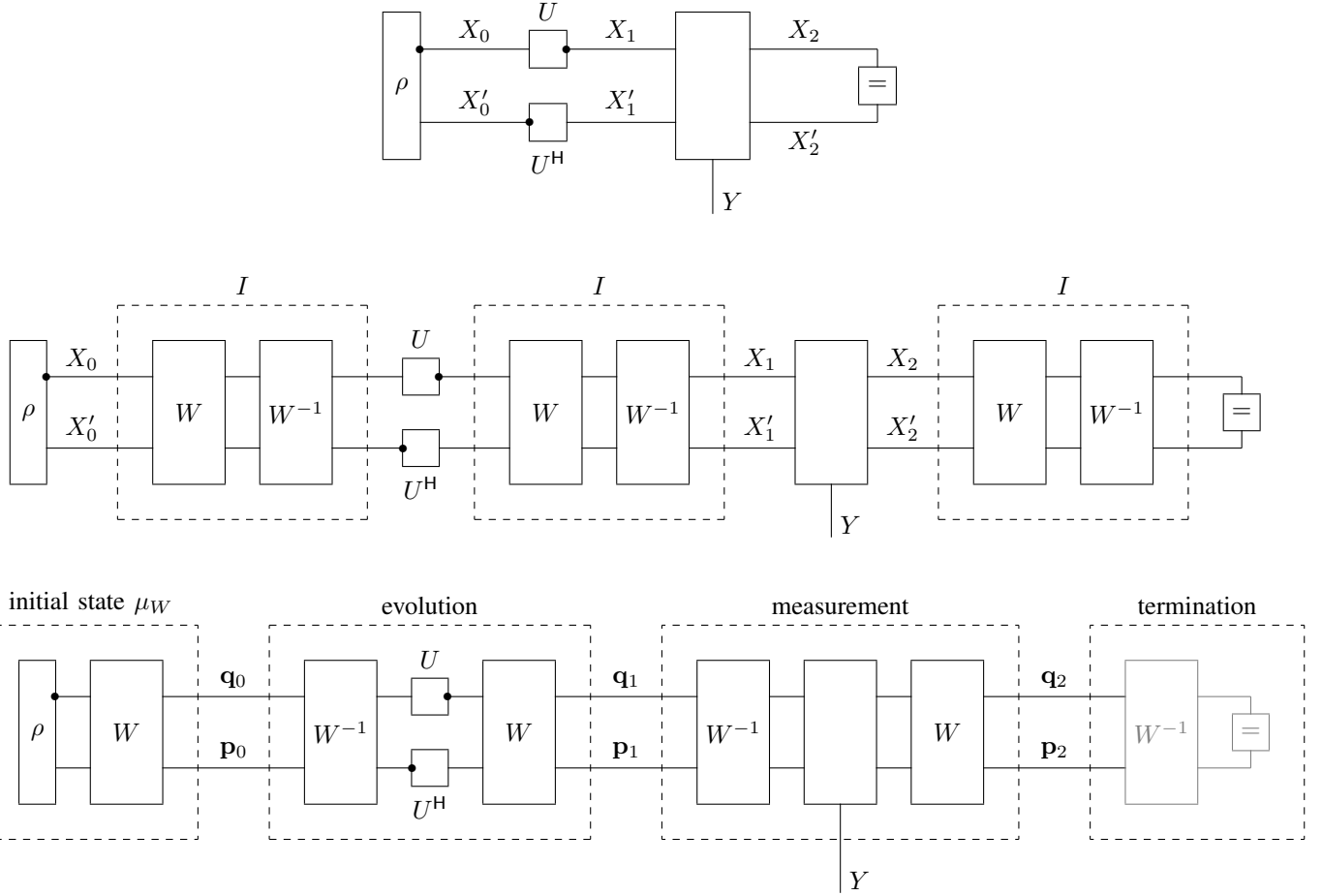


Fig. 63. Wigner-Weyl transform of a quantum factor graph with W as defined in Fig. 64. Top: quantum system with a single measurement yielding Y . Middle: inserting neutral factors (identity operators) $I = WW^{-1}$ does not change the exterior function $p(y)$. Bottom: closing the dashed boxes yields the factor graph of the Wigner-Weyl representation. The termination box reduces to an empty box.

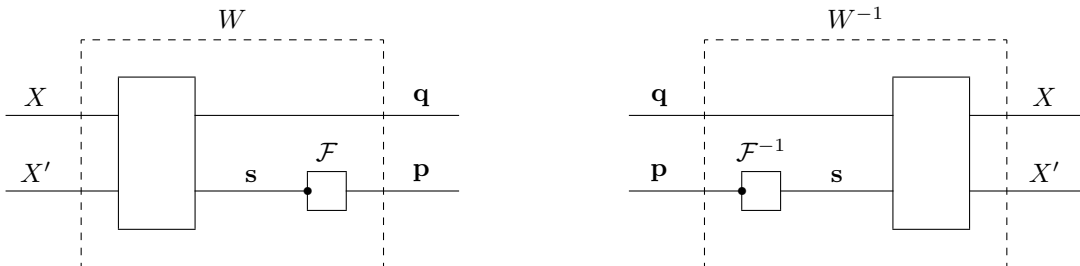


Fig. 64. Factor graphs of Wigner-Weyl transformation operator W (left) and its inverse (right). The unlabeled box inside W represents the factor (81); the unlabeled box inside W^{-1} represents the factor (83).

variables, i.e., the sum in (5) and (6) is replaced by an integral. Moreover, the equality constraint function (9) becomes

$$f = (x_1, \dots, x_n) = \delta(x_1 - x_2) \cdots \delta(x_{n-1} - x_n), \quad (77)$$

where δ is the Dirac delta. Finally, matrices (cf. Section II-B) are generalized to operators, i.e., the sums in (11) and (12) are replaced by integrals.

The transformation to the Wigner–Weyl representation uses an operator W that will be described below. Factor graphs for the Wigner–Weyl representation may then be obtained from the factor graphs in Sections III–V by a transformation as in Fig. 63. The example in this figure is a factor graph as in Fig. 25 with a single measurement, but the generalization to any number of measurements is obvious. Starting from the original factor graph (top in Fig. 63), we first insert neutral factors (identity operators) factored as $I = WW^{-1}$ as shown in Fig. 63 (middle); clearly, this manipulation does not change $p(y)$. We then regroup the factors as in Fig. 63 (bottom), which again leaves $p(y)$ unchanged. The Wigner–Weyl factor graph is then obtained by closing the dashed boxes in Fig. 63 (bottom). (The Wigner–Weyl representation has thus been obtained as a “holographic” factor graph transform as in [27], [28].)

The operator W encodes the relations

$$X = \mathbf{q} - \mathbf{s} \quad (78)$$

$$X' = \mathbf{q} + \mathbf{s} \quad (79)$$

and the Fourier transform with kernel

$$\mathcal{F}(\mathbf{s}, \mathbf{p}) = \left(\frac{1}{\pi\hbar} \right)^N e^{(i/\hbar)2\mathbf{p}^T \mathbf{s}}. \quad (80)$$

For the purpose of this paper, \hbar (the reduced Planck constant) is an arbitrary scale factor.

The factor-graph representation of the operator W (shown left in Fig. 64) consists of two factors: the first factor is

$$\delta(x - (\mathbf{q} - \mathbf{s})) \delta(x' - (\mathbf{q} + \mathbf{s})), \quad (81)$$

which encodes the constraints (78) and (79); the second factor is the Fourier kernel (80).

The factor-graph representation of W^{-1} (right in Fig. 64) consists of the inverse Fourier transform kernel

$$\mathcal{F}^{-1}(\mathbf{s}, \mathbf{p}) = e^{(-i/\hbar)2\mathbf{p}^T \mathbf{s}} \quad (82)$$

and the factor

$$\delta\left(\mathbf{q} - \frac{1}{2}(x + x')\right) \delta\left(\mathbf{s} - \frac{1}{2}(-x + x')\right). \quad (83)$$

Closing the “initial state” box in Fig. 63 yields the function

$$\mu_W(\mathbf{q}, \mathbf{p}) = \int_{-\infty}^{\infty} \left(\frac{1}{\pi\hbar} \right)^N e^{(i/\hbar)2\mathbf{p}^T \mathbf{s}} \rho(\mathbf{q} - \mathbf{s}, \mathbf{q} + \mathbf{s}) ds \quad (84)$$

for $\mathbf{q} = \mathbf{q}_0$ and $\mathbf{p} = \mathbf{p}_0$, which is easily seen to be real (since $\rho(x, x') = \rho(x', x)$).

Closing the “termination” box in Fig. 63 yields the function

$$\int_{-\infty}^{\infty} \int_{-\infty}^{\infty} \int_{-\infty}^{\infty} e^{(-i/\hbar)2\mathbf{p}^T \mathbf{s}} \delta\left(\mathbf{q} - \frac{1}{2}(x + x')\right) \delta\left(\mathbf{s} - \frac{1}{2}(-x + x')\right) \delta(x - x') dx' dx ds$$

$$= \int_{-\infty}^{\infty} e^{(-i/\hbar)2\mathbf{p}^T \mathbf{s}} \delta(\mathbf{s}) ds \quad (85)$$

$$= 1. \quad (86)$$

The termination box thus reduces to an empty box and can be omitted.

APPENDIX C MONTE CARLO METHODS

Let $f(x_1, \dots, x_n)$ be a nonnegative real function of finite-alphabet variables x_1, \dots, x_n . Many quantities of interest in statistical physics, information theory, and machine learning can be expressed as a partition sum

$$Z_f \triangleq \sum_{x_1, \dots, x_n} f(x_1, \dots, x_n) \quad (87)$$

of such a function f . The numerical computation of such quantities is often hard. When other methods fail, good results can sometimes be obtained by Monte Carlo methods [40]–[42]. A key quantity in such Monte Carlo methods is the probability mass function

$$p_f(x_1, \dots, x_n) \triangleq f(x_1, \dots, x_n)/Z_f. \quad (88)$$

An extension of such Monte Carlo methods to functions f that can be negative or complex was outlined in [43]. However, only the real case (where f can be negative) was addressed in some detail in [43]. We now substantiate the claim from [43] that complex functions q as represented by the factor graphs of this paper can be handled as in the real case.

We will use the abbreviation $x \triangleq (x_1, \dots, x_n)$, and, following [43], we define

$$Z_{|f|} \triangleq \sum_x |f(x)| \quad (89)$$

and the probability mass function

$$p_{|f|}(x) \triangleq \frac{|f(x)|}{Z_{|f|}} \quad (90)$$

Note that $p_{|f|}$ inherits factorizations (and thus factor graphs) from f . This also applies to more general distributions of the form

$$p(x; \rho) \propto |f(x)|^\rho \quad (91)$$

for $0 < \rho < 1$.

For the real case, the gist of the Monte Carlo methods of [43] is as follows:

- 1) Generate a list of samples $x^{(1)}, \dots, x^{(K)}$ either from $p_{|f|}(x)$, or from a uniform distribution over x , or from an auxiliary distribution $p(x; \rho)$ as in (91).
- 2) Estimate Z (and various related quantities) from sums such as

$$\sum_{k: f(x^{(k)}) > 0} f(x^{(k)}) \quad (92)$$

and

$$\sum_{k:f(x^{(k)})<0} f(x^{(k)}), \quad (93)$$

or

$$\sum_{k:f(x^{(k)})>0} \frac{1}{f(x^{(k)})} \quad (94)$$

and

$$\sum_{k:f(x^{(k)})<0} \frac{1}{f(x^{(k)})}, \quad (95)$$

or, more generally,

$$\sum_{k:f(x^{(k)})>0} \frac{f(x^{(k)})^{\rho_1}}{f(x^{(k)})^{\rho_2}} \quad (96)$$

and

$$\sum_{k:f(x^{(k)})<0} \frac{f(x^{(k)})^{\rho_1}}{f(x^{(k)})^{\rho_2}} \quad (97)$$

The idea is always that the sampling probability equals the denominator (up to a scale factor), which results in simple expectations for these sums. (The quantities (96) and (97) are not actually mentioned in [43], but they arise from translating multi-temperature Monte Carlo methods (cf. [41], [42]) to the setting of [43].)

Note that Step 1 above (the generation of samples) generalizes immediately to the complex case; our issue here is Step 2, where the generalization is less obvious.

Recall now that all factor graphs in Sections III–V represent functions with the structure

$$q(x, x', y) = g(x, y) \overline{g(x', y)} \quad (98)$$

as in Fig. 13. But any such function satisfies

$$q(x, x', y) = \overline{q(x', x, y)}. \quad (99)$$

Under any of the probability distributions in Step 1 above, a configuration (x, x', y) then has the same probability as the conjugate configuration (x', x, y) (i.e., (x, x', y) and (x', x, y) are so-called antithetic variates). We can thus double the list of samples in Step 1 by adding all the conjugate configurations. For the augmented list of samples, the sum (92) becomes

$$\sum_{k:f(x^{(k)})+\overline{f(x^{(k)})}>0} f(x^{(k)}) + \overline{f(x^{(k)})}, \quad (100)$$

and the sums (93)–(97) can be handled analogously.

ACKNOWLEDGMENT

The material of this paper has been developing over a long time. Its beginnings have benefitted from discussions, mostly long ago, with Niclas Wiberg, Justin Dauwels, Frank Kschischang, and Nikolai Nefedov. More recently, we have profited from discussions with Ali Al-Bashabsheh, G. David Forney, Jr., and Yongyi Mao. We also thank the reviewers of [1] and Alexey Kovalev for pointing out pertinent work in the physics literature.

REFERENCES

- [1] H.-A. Loeliger and P. O. Vontobel, “A factor-graph representation of probabilities in quantum mechanics,” *Proc. 2012 IEEE Int. Symp. on Information Theory*, Cambridge, MA, USA, July 1–6, 2012, pp. 656–660.
- [2] F. R. Kschischang, B. J. Frey, and H.-A. Loeliger, “Factor graphs and the sum-product algorithm,” *IEEE Trans. Inf. Theory*, vol. 47, pp. 498–519, Feb. 2001.
- [3] G. D. Forney, Jr., “Codes on graphs: normal realizations,” *IEEE Trans. Inf. Theory*, vol. 47, no. 2, pp. 520–548, 2001.
- [4] H.-A. Loeliger, “An introduction to factor graphs,” *IEEE Sig. Proc. Mag.*, Jan. 2004, pp. 28–41.
- [5] M. Mézard and A. Montanari, *Information, Physics, and Computation*. Oxford University Press, 2009.
- [6] M. I. Jordan, “Graphical models,” *Statistical Science*, vol. 19, no. 1, pp. 140–155, 2004.
- [7] Ch. M. Bishop, *Pattern Recognition and Machine Learning*. New York: Springer Science+Business Media, 2006.
- [8] D. Koller and N. Friedman, *Probabilistic Graphical Models*. Cambridge, MA, MIT Press, 2009.
- [9] T. Richardson and R. Urbanke, *Modern Coding Theory*. Cambridge University Press, 2008.
- [10] H. Wymeersch, *Iterative Receiver Design*. Cambridge University Press, 2007.
- [11] H.-A. Loeliger, J. Dauwels, Junli Hu, S. Korl, Li Ping, and F. R. Kschischang, “The factor graph approach to model-based signal processing,” *Proceedings of the IEEE*, vol. 95, no. 6, pp. 1295–1322, June 2007.
- [12] H.-A. Loeliger, L. Bruderer, H. Malmberg, F. Wadehn, and N. Zalmai, “On sparsity by NUV-EM, Gaussian message passing, and Kalman smoothing,” 2016 Information Theory & Applications Workshop (ITA), La Jolla, CA, Jan. 31 – Feb. 5, 2016.
- [13] P. O. Vontobel, “The Bethe permanent of a non-negative matrix,” *IEEE Trans. Inf. Theory*, vol. 59, pp. 1866–1901, Mar. 2013.
- [14] M. Veltman, *Diagrammatica: The Path to Feynman Diagrams*. Cambridge Lecture Notes in Physics, 1994.
- [15] Z.-C. Gu, M. Levin, and X.-G. Wen, “Tensor-entanglement renormalization group approach as a unified method for symmetry breaking and topological phase transitions,” *Phys. Rev. B*, vol. 78, p. 205116, Nov. 2008.
- [16] J. I. Cirac and F. Verstraete, “Renormalization and tensor product states in spin chains and lattices,” *J. Phys. A: Math. and Theor.*, vol. 42, no. 504004, pp. 1–34, 2009.
- [17] B. Coecke, “Quantum picturalism,” *Contemporary Phys.*, vol. 51, no. 1, pp. 59–83, 2010.
- [18] C. J. Wood, J. D. Biamonte, and D. J. Cory, “Tensor networks and graphical calculus for open quantum systems,” *Quantum Information and Computation*, vol. 15, pp. 759–811, 2015.
- [19] M. A. Nielsen and I. L. Chuang, *Quantum Computation and Quantum Information*. Cambridge University Press, 2000.
- [20] R. Mori, “Holographic transformation, belief propagation and loop calculus for generalized probabilistic theories,” *Proc. 2015 IEEE Int. Symp. on Information Theory*, Hong Kong, China, June 14–19, 2015.
- [21] R. R. Tucci, “Quantum information theory – a quantum Bayesian net perspective,” arXiv:quant-ph/9909039v1, 1999.
- [22] M. S. Leifer and D. Poulin, “Quantum graphical models and belief propagation,” *Annals of Physics*, vol. 323, no. 8, pp. 1899–1946, Aug. 2008.
- [23] M. X. Cao and P. O. Vontobel, “Estimating the information rate of a channel with classical input and output and a quantum state,” submitted to 2017 IEEE Int. Symp. on Information Theory. Available from http://www.ie.cuhk.edu.hk/~vpascal/students/cao_vontobel_isit2017_subm1.pdf
- [24] P. O. Vontobel and H.-A. Loeliger, “On factor graphs and electrical networks,” in *Mathematical Systems Theory in Biology, Communication, Computation, and Finance*, J. Rosenthal and D. S. Gilliam, eds., IMA Volumes in Math. & Appl., Springer Verlag, 2003, pp. 469–492.
- [25] P. Cvitanović, *Group Theory: Birdtracks, Lie's, and Exceptional Groups*. Princeton Univ. Press, 2008.
- [26] E. Peterson, “Unshackling linear algebra from linear notation,” arXiv:0910.1362, 2009.
- [27] A. Al-Bashabsheh and Y. Mao, “Normal factor graphs and holographic transformations,” *IEEE Trans. Inf. Theory*, vol. 57, no. 2, pp. 752–763, Feb. 2011.
- [28] G. D. Forney, Jr., and P. O. Vontobel, “Partition functions of normal factor graphs,” *Proc. Inf. Theory & Appl. Workshop*, UC San Diego, La Jolla, CA, USA, Feb. 6–11, 2011.

- [29] A. Al-Bashabsheh, Y. Mao, and P. O. Vontobel, "Normal factor graphs: a diagrammatic approach to linear algebra," *Proc. IEEE Int. Symp. Inf. Theory*, St. Petersburg, Russia, Jul. 31–Aug. 5, 2011, pp. 2178–2182.
- [30] W. H. Zurek, "Decoherence, einselection, and the quantum origins of the classical," *Rev. Mod. Phys.*, vol. 75, no. 3, pp. 715–775, July 2003.
- [31] W. H. Zurek, "Quantum Darwinism," *Nature Physics*, vol. 5, pp. 181–188, March 2009.
- [32] H.-P. Breuer and F. Petruccione, *Open Quantum Systems*. Oxford University Press, New York, NY, 2002.
- [33] M. Schlosshauer, "Decoherence, the measurement problem, and interpretations of quantum mechanics," *Rev. Mod. Phys.*, vol. 76, pp. 1267–1305, Oct. 2004.
- [34] R. Cowen, "Space, time, entanglement," *Nature*, vol. 527, pp. 290–293, Nov. 2015.
- [35] M. G. Parker, "Quantum factor graphs," *Ann. Télécomm.*, vol. 56, no. 7–8, pp. 472–483, 2001.
- [36] M. S. Leifer, D. Poulin, "Quantum graphical models and belief propagation," *Ann. Phys.*, vol. 323, no. 8, pp. 1899–1946, 2008.
- [37] R. van Leeuwen, N. E. Dahlen, G. Stefanucci, C.-O. Almbladh, and U. van Barth, "Introduction to the Keldysh formalism," *Lect. Notes Phys.*, vol. 706, pp. 33–59, 2006.
- [38] P. O. Vontobel, "A factor-graph approach to Lagrangian and Hamiltonian dynamics," *Proc. IEEE Int. Symp. Information Theory*, St. Petersburg, Russia, Jul. 31 – Aug. 5, 2011, pp. 2183–2187.
- [39] R. P. Feynman and A. R. Hibbs, *Quantum Mechanics and Path Integrals*. New York: McGraw-Hill, 1965.
- [40] D. J. C. MacKay, "Introduction to Monte Carlo methods," in *Learning in Graphical Models*, M. I. Jordan, ed., Kluwer Academic Press, 1998, pp. 175–204.
- [41] R. M. Neal, *Probabilistic Inference Using Markov Chain Monte Carlo Methods*, Techn. Report CRG-TR-93-1, Dept. Comp. Science, Univ. of Toronto, Sept. 1993.
- [42] M. Molkaraie and H.-A. Loeliger, "Monte Carlo algorithms for the partition function and information rates of two-dimensional channels," *IEEE Trans. Inf. Theory*, vol. 59, no. 1, pp. 495–503, Jan. 2013.
- [43] M. Molkaraie and H.-A. Loeliger, "Extending Monte Carlo methods to factor graphs with negative and complex kernels," *Proc. 2012 IEEE Information Theory Workshop*, Lausanne, Switzerland, Sept. 3–7, 2012, pp. 367–371.